EFFECTS OF DIESEL—WATER EMULSION COMBUSTION ON DIESEL ENGINE NO_x EMISSIONS

By

C. ALAN CANFIELD

A THESIS PRESENTED TO THE GRADUATE SCHOOL OF THE
UNIVERSITY OF FLORIDA IN PARTIAL FULFILLMENT
OF THE REQUIREMENTS FOR THE DEGREE OF
MASTER OF SCIENCE

UNIVERSITY OF FLORIDA

1999

ACKNOWLEDGEMENTS

I owe thanks to many individuals for supporting me in my graduate studies at the University of Florida (UF) while working full-time. I extend special and sincere thanks to my advisor and committee chair, Dr. Zhuomin Zhang, for providing valuable advice in the thesis preparation and graduate studies. Additional thanks go to Dr. Charles Proctor, III, for guidance in establishing the thesis proposal and background review, and Drs. William Lear and Alex Green for serving on my committee.

All graduate coursework was conducted through the distance learning program facilitated by the Florida Engineering Education and Delivery System (FEEDS) offices at UF and the Florida State University Panama City Campus (FSU/PCC). I sincerely appreciate the dedication and patience of Professors Hsieh, Zhang, Mittal, and Kurzweg for accommodating off-campus students in their courses. Ms. Becky Hoover of the UF Mechanical Engineering Graduate Office, Ms. Joyce Phillips of the UF FEEDS office, and Ms. Pat Lawson of the FSU/PCC FEEDS office were invaluable in course administration. Mr. Oliver Canaday of the Tyndall AFB Education Center and Ms. Sheila Ray of the Tyndall AFB Library supported the receipt and viewing of my course videotapes. Without the support of these individuals, I would not have been able to pursue or complete this program.

I gratefully acknowledge and value the long-term support and friendship of Dr. Joe Wander of the Air Force Research Lab, Airbase & Environmental Technology Division. Dr. Aly Shaaban of Applied Research Associates graciously provided testing data for evaluation. Finally, I dedicate this thesis to my parents, Charles and Katherine Canfield.

PREFACE

This thesis is the result of graduate studies and research toward a Master of Science in mechanical engineering at the University of Florida. The coursework and research was conducted while working full-time for Applied Research Associates, Inc. at Tyndall Air Force Base, Florida, supporting the Air Force Research Laboratory (AFRL) Airbase & Environmental Technology Division. Dr. Joseph D. Wander was the Air Force Project Officer.

Most of the test data evaluated in this thesis was collected by Dr. Aly Shaaban in 1996, with the remainder collected in late 1998 by the author. A project to implement the alternative fuel described herein for a six-month test is planned for early 1999. A patent application is under review for the additive package used for maintaining a stable fuel—water mixture, preventing detailed description of the additive components.

TABLE OF CONTENTS

page

ABBREVIATIONS

AFB	Air Force Base
AGE	aerospace ground equipment
ARB	Air Reserve Base
BDC	bottom dead center
BSFC	brake specific fuel consumption
CI	compression ignition
CN	cetane number
CO	carbon monoxide
CR	compression ratio
EPA	Environmental Protection Agency
HC	hydrocarbon
ICE	internal combustion engine
MIL-SPEC	military specification
NO_x	nitrogen oxides
NO	nitric oxide
NO_2	nitrogen dioxide
SI	spark ignition
SVOC	semi-volatile organic compound
TDC	top dead center
UHC	unburned hydrocarbons
USAF	United States Air Force
VOC	volatile organic compound

Abstract of Thesis Presented to the Graduate School
of the University of Florida in Partial Fulfillment of the
Requirements for the Degree of Master of Science

EFFECTS OF DIESEL—WATER EMULSION COMBUSTION ON DIESEL ENGINE NO_x EMISSIONS

By

C. Alan Canfield

May 1999

Chairman: Zhuomin Zhang
Major Department: Mechanical Engineering

This study examines the effects of combusting a mixture of diesel fuel, water, and surfactant on the nitrogen oxides, or NO_x, emissions from a compression ignition diesel engine. Previous research has attributed the observed reduction of nitrogen oxide emissions to a suppression of flame temperature due to quenching effects from the water, thereby reducing thermal NO_x formation. The thesis highlights the relevant theory, operation, and design parameters of diesel internal combustion engines. Experimental procedures conducted using a Detroit Diesel 4-cyclinder diesel engine are discussed. Results from testing diesel fuel with varying ratios of water balanced with a surfactant to stabilize the emulsion will be presented and discussed. The data shows significant NO_x emission reduction with up to 45 percent water, by volume, in the fuel. These results are correlated with a thermodynamic first law analysis to estimate the adiabatic flame temperature of the standard fuel and fuel—water emulsion cases. Results indicate that thermal NO_x is indeed reduced by quenching and flame temperature suppression, confirming reports in the literature. Recommendations are given for further studies, including improving the fuel—water emulsion and considerations for long-term testing.

CHAPTER 1

INTRODUCTION

Background

McClellan Air Force Base (AFB), California, identified mobile diesel engines as contributing nearly as much total NO_x emissions as aircraft and stationary sources combined. Hourly-rated diesel engines contributed 75 percent of this NO_x, with the remainder emitting from gasoline and diesel engines rated in miles (Canfield et al., 1997). Hourly-rated diesel engines include non-road mobile equipment such as forklifts, bulldozers, air-conditioning units, and generators. McClellan AFB is located in Sacramento, California, classified as Extreme for ozone attainment status. This classification recognizes ozone pre-cursors, NO_x and VOCs, as immediately dangerous to human and environmental health, and places the highest restrictions on emissions and fines for exceeding these limits.

In addition to air quality compliance concerns at McClellan AFB, March Air Reserve Base (ARB) in southern California faced immediate reduction in training and operational use of AGE generators due to South Coast Air Quality Management District (SCAQMD) Rule 1110.2. This

Table 1: Regulatory emission limits and emissions from A/M32A-86

Air pollutant	Rule 1110.2 limit, ppm	A/M32A emissions by load, ppm		
		18 kW(e)	36 kW(e)	72 kW(e)
NO_x	36	761	1171	2118
CO	2000	54	47	95

rule placed regulatory limits on emissions from non-road mobile sources over 37 kW. These limits, and the corresponding emissions from an A/M32A-86 diesel generator at varying electric generator loads, are listed in Table 1. The A/M32A-86 generator, the subject of the present study, is described in detail in Chapter 4. Please note in Table 1 the limit of 36 ppm for NO_x emissions, while the A/M32A-86 emits over 20 times this at 18 kW, only 25 percent of full load.

AGE does not currently meet these emission limitations and will not without emission controls and/or combustion system or fuel modifications. All AGE units over 50 hp were required to comply with Rule 1110.2 emission limits by 31 Dec 94 or the facility would: 1) remove the AGE units from service, 2) pay daily fines, 3) or submit a proposal for complete electrification by Dec 1999.

AGE at March ARB fell under three general categories:

1. Gasoline-fueled internal combustion engines (ICEs)
2. Diesel-fueled ICEs
3. JP-8-fueled turbine engines

There were 81 total pieces of AGE over 37 kW, excluding turbine-powered AGE, at March ARB in 1996. The 168 units of AGE under 37 kW are not presently regulated by Rule 1110.2.

The Air Force surveyed its laboratories for potential solutions to air pollutant emissions from AGE. A team was formed to investigate commercial off-the-shelf (COTS) products or developing technologies for emission controls or alternate power sources applicable to AGE. Laboratories with promising technologies were tasked to prepare preliminary and final proposals for demonstration, validation, and implementation of their technologies. A request for information was also posted in the Commerce Business Daily to survey COTS for AGE emission controls.

Several technologies proposed by the Air Force laboratories to control NO_x emissions from AGE included selective catalytic reduction, increasing O_2 in the intake air, a mobile filter cart, a

nonthermal plasma reactor control system, and water injection with the fuel, described in this thesis.

Dryer (1976) reports a reference to water injection in a combustion system dating back to 1791, in which water was used to cool the blades in early gas turbines. In the last 20 years water has received varying levels of interest as a means to improve combustion efficiency and reduce air pollutant emissions from ICEs. These reports in the literature will be discussed and compared with the current research.

Early work demonstrated that with fuel:water volumetric ratios from 1:1 to 9:1, the addition of 1-2 volume percent surfactant allowed a stable emulsion to be maintained with the diesel and water mixture. Using this formula and testing varying ratios of fuel and water for combustion properties developed the data sets that will be evaluated in this thesis. Various injector timing setting were also evaluated. For a given injector timing setting, data will be presented for the baseline case of the generator operating on standard military diesel, and for various fuel mixtures of different water volume ratios.

Objective

The purpose of this research is to investigate the use of a stabilized diesel—water fuel mixture as a drop-in replacement in U.S. Air Force (USAF) mobile aerospace ground equipment (AGE). The USAF is interested in lowering the emissions of nitrogen oxides (NO_x) and other emissions from AGE during training and non-warfighting missions to comply with air quality regulations governing facilities in the continental United States.

The tasks involved in this research involved (1) evaluating the performance and behavior of the fuel—water mixtures and (2) measuring the effect of the fuel—water mixture on AGE power and air pollutant emissions. Previous unpublished work at the author's laboratory determined the optimal diesel—water emulsion preparation techniques and mixture ratios. Research reported

herein focused on evaluating varying ratios of water in the fuel and the resultant effect on air pollutant emissions, especially NO_x.

This study was conducted as part of an Air Force initiative to reduce emissions from aerospace ground equipment (Akridge et al., 1997, and Canfield et al., 1997). Of six technologies evaluated for AGE NO_x reduction, the fuel—water emulsion promises the easiest "drop-in" solution. NO_x emissions can be lowered with little or no modifications required to the diesel engines.

Outline

This thesis begins with a review internal combustion engines in Chapter 2, including history, physical components and geometry, and mass and heat transfer aspects. Chapter 3 will discuss internal combustion engine air pollutant formation pathways and existing control technology options. The test engine, experimental procedures, fuel properties and variables, and data collection will be described in Chapter 4. Chapter 5 will present the experimental data and results, with a comparison to first law of thermodynamics and equilibrium products code predictions. NOx formation rate equations will be presented in Chapter 5, and the potential effects of water injection on combustion will be described. Chapter 6 will discuss the findings, conclusions, and recommendations from the research, including confirmation of research published in the literature.

CHAPTER 2

REVIEW OF INTERNAL COMBUSTION ENGINE FUNDAMENTALS

History of Internal Combustion Engines

From the first application of open fire to provide heating, lighting, and cooking, combustion science has evolved to providing distributed electricity generation and mechanical energy for most modes of transportation. Combustion is described as either external or internal. External combustion is defined as combustion in which the process fluid is external to, or different from, the mechanical energy-producing fluid. For example, coal-fired power plants operate as external combustion because the coal is combusted to generate steam, and the steam then turns a turbine to generate electricity. If the fluid undergoing combustion also generates mechanical energy in the system, the process is defined as internal combustion. For example, in reciprocating internal combustion engines the gas expansion from combustion of the air and fuel mixture moves a piston, which turns a crankshaft, generating mechanical power for propulsion, electricity generation, etc. Gas turbines and rocket engines are also defined as internal combustion, since, in both cases, the air and fuel mixtures after combustion and compression provide mechanical power through thrust.

Advances in the understanding of the thermodynamic cycles of combustion have improved the design of combustion engines. Improvements in materials science also support improvements in engine performance and durability. For example, advances in materials and design have improved the compressor ratio of gas turbines from 3:1 to 30:1, and increased the efficiencies from 3.5% to 30%. Similarly, computer modeling and simulation has supported advanced intake,

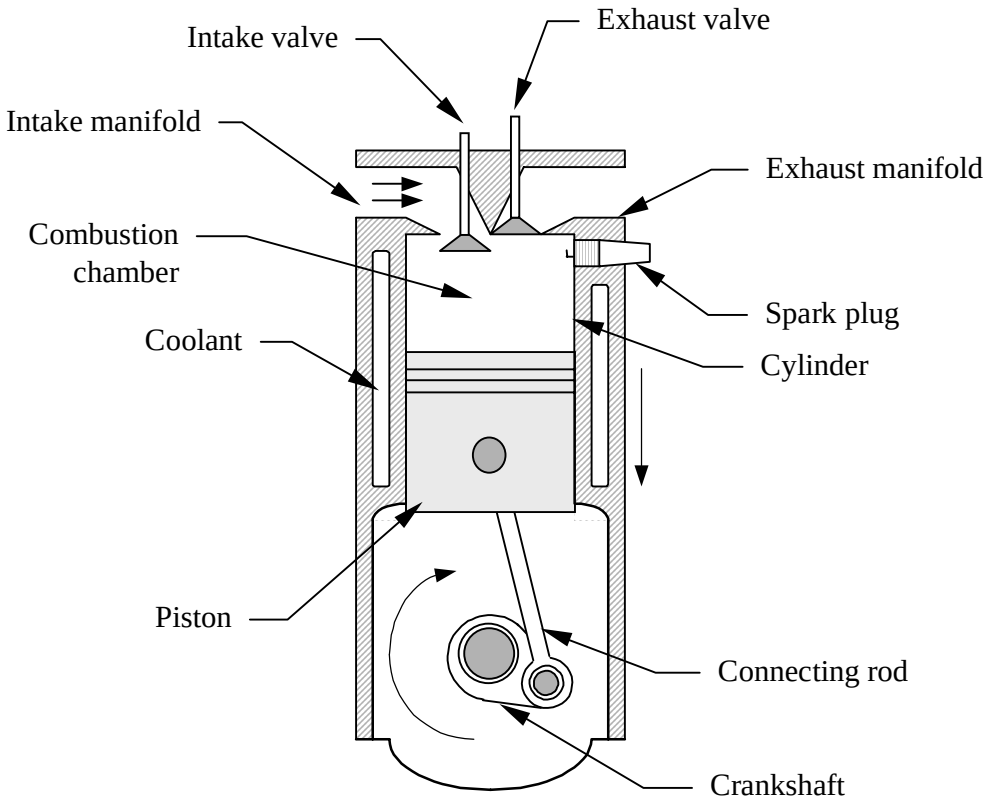

Figure 1: Spark-ignition engine cross-section

combustion cylinder, and exhaust systems design on modern automobiles resulting in higher thermal and mechanical efficiencies with reduced air pollutant emissions.

Physical Engine Characteristics

Before discussing the operation, design, and analysis of internal combustion engines (ICEs), it is worthwhile to review the specific engine components involved in and affecting the combustion process. Figure 1 shows a cross-section of a spark ignition, two-stroke engine. Important characteristics of the internal combustion engine are listed in Table 2.

Critical to evaluating the performance of an ICE are quantities derived from the geometry of the combustion cyclinder and the motion of the piston in the cylinder. A simplified piston,

Table 2: Physical engine components

Component	Description and Function
Cylinder	Channel of circular cross-section bored into the engine block in which a piston moves linearly in a reciprocating motion
Piston	Cylindrical component riding back and forth in the engine cylinder converting the thermal energy released by the combustion process into mechanical energy
Crankshaft	Shaft with offsets to hold the piston connecting rod and translate linear piston motion to circular motion
Combustion chamber	Portion of the cylinder enclosed by the piston and the head of the cylinder. When the piston reaches the top or extent of motion into the cylinder and combustion of the fuel-air mixture occurs, the themal energy released raises the pressure in the combustion chamber and forces the piston back.
Intake manifold	The collection of pipes carrying air (fuel injected) or air and fuel (carbureted) to the engine inlet valves.
Exhaust manifold	Collection of pipes carrying the combusted air/fuel mixture away from the engine.
Inlet valves	Poppet valves that control the introduction of air or air and fuel into the engine combustion chamber.
Exhaust valves	Poppet valves that control the release of combusted air/fuel mixture to the exhaust system.
Spark plug	Electrode protruding into the combustion chamber. A high-voltage arc is passed across an electrode to provide ignition in the lower-compression spark ignition engines.

cylinder, connecting rod, and crankshaft are shown in Figure 2. The compression ratio, *CR*, is the ratio of the maximum cylinder volume to minimum cylinder volume,

$$CR = \frac{V_s + V_c}{V_c} \tag{1}$$

where V_c is the cylinder clearance volume, cm^3, and V_s is the cylinder swept volume, cm^3. The cylinder volume at any crank position θ is given by

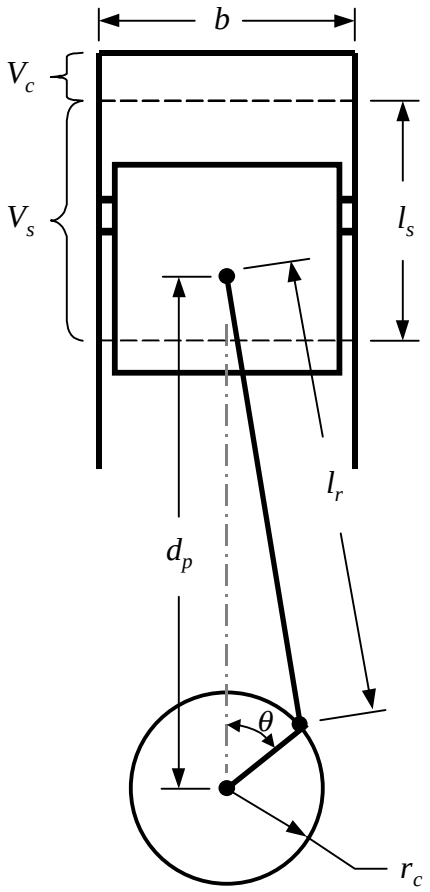

b = cylinder bore, cm
V_c = clearance volume, cm^3
V_s = swept volume, cm^3
l_s = stroke length, cm
TDC = top dead center
BDC = bottom dead center
d_p = distance from piston pivot axis to crank axis, cm
l_r = connecting rod length, cm
θ = crank angle, rad
r_c = crankshaft radius, cm

Figure 2: Reciprocating ICE geometry (not to scale)

$$V_s = V_c + \frac{\pi b^2}{4}\left(l_r + r_c - d_p\right). \tag{2}$$

Please refer to Figure 2 for additional ICE geometry nomenclature. The stroke length, l_s, and the cylinder bore, b, are critical in determining the power output of the combustion process.

ICE Thermodynamic Cycles

Combustion in reciprocating piston ICEs is commonly assumed to operate either as a constant volume or constant pressure process. The Otto cycle, a constant volume heat addition thermodynamic process, closely models combustion in spark ignition (SI) ICEs. The diesel cycle is a constant pressure, slower-speed cycle depicting combustion in compression ignition, or diesel, cycle engines. A combination of the Otto and diesel cycles is referred to as the mixed,

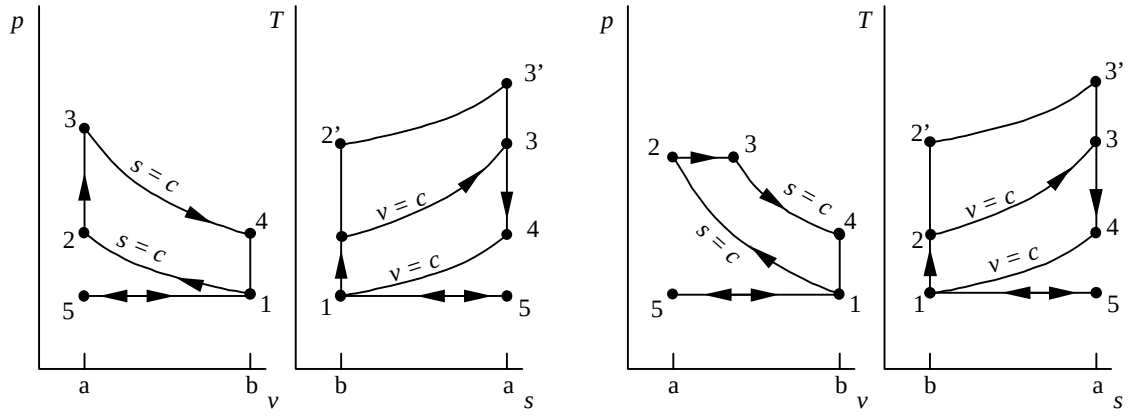

$5 \rightarrow 1$: Suction, air intake
$1 \rightarrow 2$: Adiabatic compression
$2 \rightarrow 3$: Constant volume heat addition
$3 \rightarrow 4$: Adiabatic expansion
$4 \rightarrow 1$: Constant volume heat rejection
$1 \rightarrow 5$: Exhaust to atmosphere

Otto Cycle

$5 \rightarrow 1$: Suction, air intake
$1 \rightarrow 2$: Adiabatic compression
$2 \rightarrow 3$: Constant pressure heat addition
$3 \rightarrow 4$: Adiabatic expansion
$4 \rightarrow 1$: Constant pressure heat rejection
$1 \rightarrow 5$: Exhaust to atmosphere

Diesel Cycle

Figure 3: Ideal air-standard Otto and diesel cycles

limited pressure, or combination cycle. The Otto and diesel cycles are shown in Figure 3 to demonstrate the differences. As mentioned, the constant volume heat addition of the Otto cycle and the constant pressure heat addition of the diesel cycle are shown in step $2 \rightarrow 3$ of the respective set of graphs. The primed points (i.e., *2'* and *3'*) depict the non-isentropic expansion points attained due to irreversibility. The label $s = c$ and $v = c$ refer to the ideal constant specific entropy and specific volume for the respective step.

The graphs shown in Figure 3 depict the theoretical, adiabatic compression and expansion of the Otto and diesel cycles. Actual combustion processes vary from theoretical due to various losses. Some of these losses are depicted in Figure 4 for the diesel, or compression ignition (CI), cycle.

Differences in Figure 4 for actual verses theoretical cycle end-points are explained below:

5' → 1: The suction stroke provides intake air to the engine cylinder for fuel oxidation. Slight losses can occur from restrictions and bends in the intake air hose, or clogging of the intake air filters. Poor intake airflow can also contribute to poor mixing of the air and atomized fuel.

1 → 2': This is the compression stroke, required for auto-ignition of the air—fuel mixture. Compression does not reach the pressure indicated at point *2* due to crevice losses and gas slippage past the piston rings.

2' → 3': This is the combustion process in which the fuel—air mixture is auto-ignited. The ideal constant-pressure heat addition shown from *2 → 3* in Figure 3 is not attained due to finite (vs. instantaneous) burning time for combustion of the fuel—air mixture.

3' → 4': The expansion process is the power stroke for the engine. Finite burning time and the effects of incomplete combustion lower the pressure attained at point *3'*. Incomplete combustion

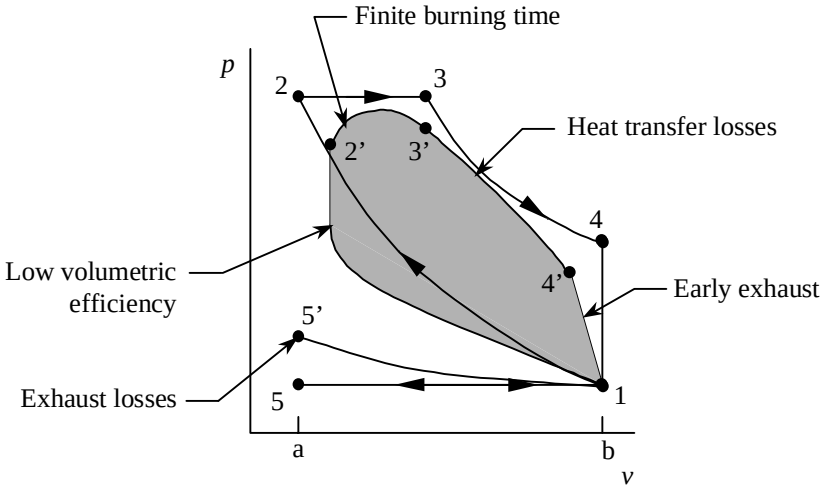

5' → 1: Suction, air intake
1 → 2': Compression
2' → 3': Ignition and combustion
3' → 4': Expansion
4' → 1: Exhaust opens
1 → 5': Exhaust to atmosphere

Figure 4. Compression ignition (diesel) cycle with losses

is a large source of losses in a CI engine, since combustion often continues during up to half of the expansion stroke . Heat transfer to the cylinder wall removes heat from the combustion gases, lowering the thermal efficiency.

4' → 1: The exhaust valves are required to open slightly before bottom-dead center (BDC) to allow sufficient time to remove all combustion by-products from the cylinder. Due to this early opening of the exhaust valves, the power stroke is complete at a lower pressure of point *4'* than ideal, shown by point *4*.

1→ 5' : Exhaust system back-pressure is the primary source of losses during exhaust. Engine power is consumed to overcome the pressure drop in the exhaust system to expel combustion products from the engine cylinder.

Spark Ignition Engines

SI automobile engines use higher-volatile gasoline as fuel and operate with compression ratios of 6:1 to 12:1, limited on the upper end by the tendency for the volatile fuels to cause "knocking." An ignition source such as a spark plug is required to initiate combustion. Compression pressures range from approximately 1000 kPa to 2000 kPa. Load and speed of the engine are controlled by throttling the fuel charge added. Several advantages include a low cost and relative weight, low starter cranking energy required, large range of speed and load, relatively high mechanical efficiency, and low specific fuel consumption. The primary disadvantages include a lower thermodynamic efficiency and high levels of air pollutant emissions across all load levels.

Compression Ignition Engines

CI engines use fuels of lower volatility, with compression ratios from 11:1 to 22:1 and compression pressures between approximately 2700 and 4800 kPa. As the name implies, the high compression pressures of the CI engine ignite the fuel/air mixture, so no ignition source (e.g., spark plug) is required. Advantages of the CI engine over the SI engine include a lower specific

fuel consumption, slightly higher thermal efficiency, relatively cheaper fuel costs, lower CO and hydrocarbon emissions at low and medium loads, lower capital costs, and higher durability. Disadvantages include higher noise of operation, higher engine weight required to withstand the higher pressures, and excess oxygen in the exhaust preventing use of standard catalysts for air pollutant control.

CI engines can be characterized by the injection type—either direct injection (DI) or indirect ignition (IDI). The Detroit Diesel 4-71N test engine is DI, implying that the fuel is injected directly into the combustion cylinder to mix with the intake air. IDI engines mix the fuel and air prior to entering the combustion cylinder in an attempt to improve mixing and therefore combustion. CI engines can additionally be characterized by the number of strokes required per power cycle, discussed below.

ICE Mechanical Cycles

Reciprocating internal combustion engines (both spark ignition and compression ignition) can be broadly characterized as four-stroke or two-stroke, depending on the number of piston strokes required for one power cycle. While the subject engine is a two-stroke compression ignition engine, it is worthwhile to describe both cycles and the inherent differences.

Four-Stroke Engine Cycle

The four-stroke engine cycle requires four piston strokes for one power cycle, which occurs with every two revolutions of the crankshaft. The step-by-step power cycle for a four-stroke ICE is shown in Figure 5. The power cycle shown is divided into intake, compression, expansion, and exhaust cycles, corresponding to steps $5 \rightarrow 1$, $1 \rightarrow 2$, $3 \rightarrow 4$, and $5 \rightarrow 1$, respectively, from the Otto cycle in Figure 3.

The inlet valve opens, allowing intake air in to the cylinder, to begin the four-stroke power cycle. The piston is moving down in the cylinder and the exhaust valve is closed. As the piston passes BDC, the inlet valve closes and the compression stroke begins. Please note Figure 5

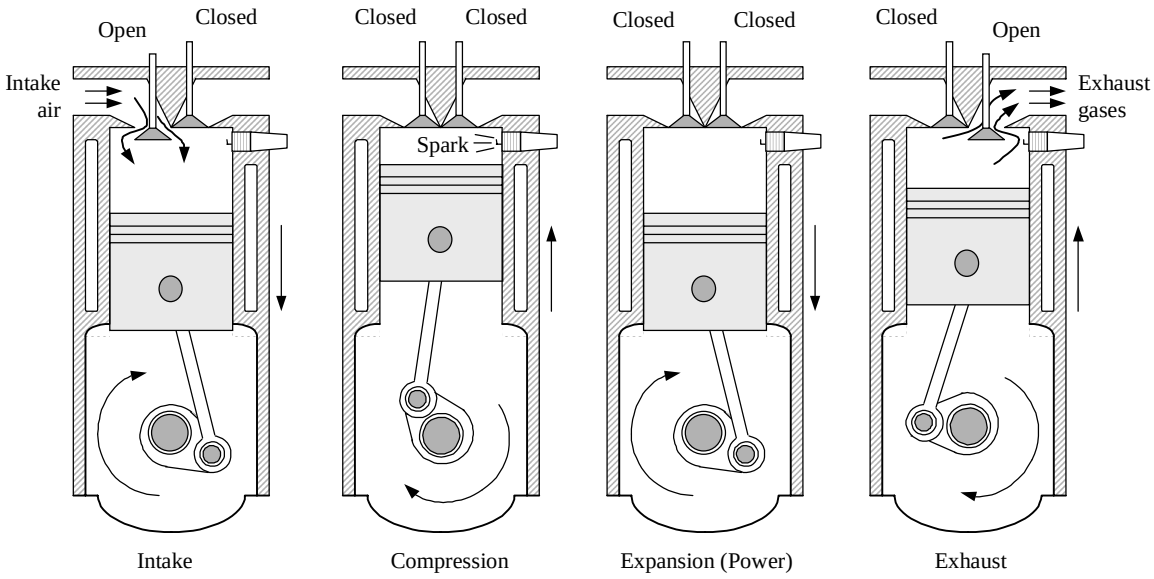

Figure 5: Four-stroke spark-ignition ICE cycle

depicts a spark ignition four-stroke cycle. A spark plug is shown applying a spark in the cylinder near the completion of the compression stroke at TDC. As mentioned earlier, spark-ignition engines require an ignition source to initiate combustion of the fuel—air mixture. A four-stroke compression ignition engine is fundamentally identical except for the lack of a spark plug, and more robust to withstand higher compression ratios.

The expansion stroke produces mechanical power from the expanding combustion gas. The inlet and exhaust valves remain closed during the compression and expansion strokes. After the piston passes BDC, the exhaust valve opens and the piston is used to drive out the combustion gas byproducts from the cylinder. This piston clearing of exhaust gases is the fundamental difference between four-stroke and two-stoke engine cycles, which are discussed next.

Two-Stroke Engine Cycle

The two-stroke engine power cycle only requires two piston strokes, or one revolution of the crankshaft. The two-stroke combustion process for the Detroit Diesel 4-71N engine, used in this study, is shown in Figure 6. During the scavenging process shown Figure 6, the exhaust valve is

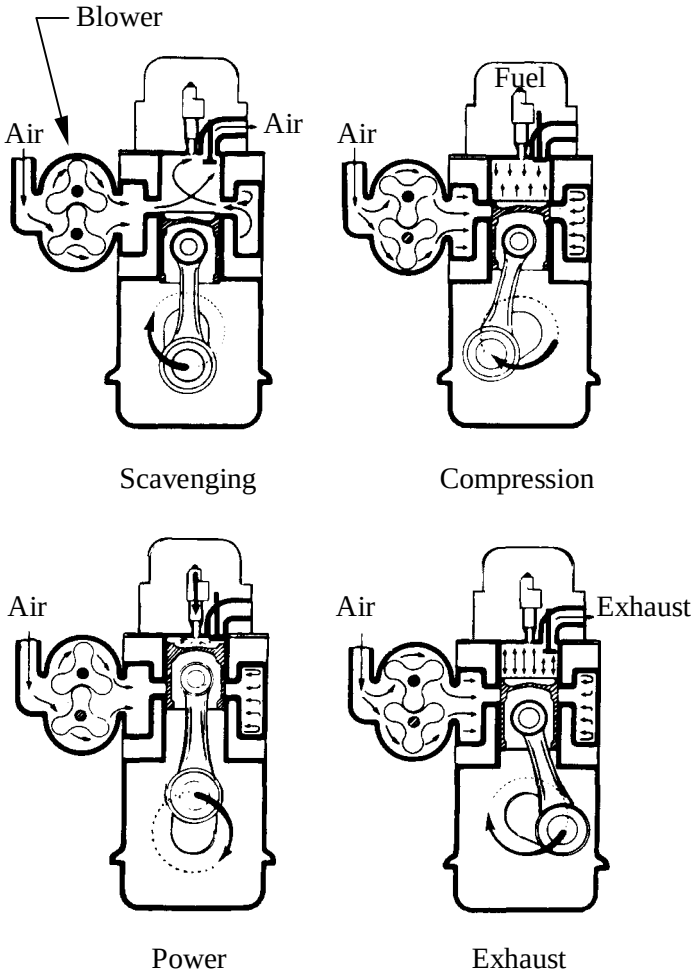

Figure 6. Detroit Diesel 4-71N two-stroke combustion process (adapted from SM-ALC/TISEA, 1986)

open and the piston is at BDC. A blower operates continuously on mechanical power from the engine. A blower is not required but improves combustion product exhaust from the cylinder. During scavenging, the blower is pushing air through slots near the bottom of the cylinder, in preparation of the compression stroke. The exhaust valve remains open to complete removal of combustion products from the cylinder.

When the compression stroke begins and the piston is rising in the cylinder, the exhaust valve is mechanically closed. Please note the lack of an intake valve: as the piston rises in the cylinder it passes and closes the intake openings. At a point designated by the injector timing setting,

atomized fuel is added to the compressing air by the fuel injector. The process is approaching the thermodynamic point *2'* in Figure 4.

When the piston reaches TDC, the fuel—air mixture is fully compressed and the mixture is auto-ignited, corresponding to step *2' → 3'* in Figure 4. The expansion (power) stroke begins, in which the expanding gas is pushing the piston down the cylinder, generating mechanical energy that is transferred to the crankshaft. The expansion (power) stroke occurs in step *2' → 3'* in Figure 4.

As the piston approaches BDC, it passes the intake slots in the bottom of the cylinder, opening the cylinder to intake air. The exhaust valve is also mechanically opened. Burned bas by-products are displaced through the exhaust valve by blower-forced intake air. The piston passes BDC and the scavenging process begins, repeating the power cycle. Note in Figure 6that the crankshaft makes only one revolution per power cycle. Recall Figure 5 depicted two revolutions and four strokes of the piston for a single power cycle.

Fuel/Air Mixtures

For practical applications combustion air can be approximated as 21% oxygen (O_2) and 79% atmospheric nitrogen (N_2). Thus, for each mole of O_2 in air there are $\frac{0.79}{0.21} = 3.76$ moles of N_2. The fuel/air equivalence ratio, ϕ, is defined as the ratio of actual fuel/air mass ratio, $(F/A)_{actual}$, to the stoichiometric fuel/air ratio, $(F/A)_s$:

$$\phi = \frac{(F/A)_{actual}}{(F/A)_s} \tag{3}$$

For $\phi = 1$, combustion is stoichiometric, for $\phi < 1$, combustion is fuel-lean (excess air is used in combustion), and for $\phi > 1$, combustion is fuel-rich. Diesel engines operate significantly fuel-lean, with typical values of $\phi = 0.8$. *F/A* is usually expressed on a mass basis as kg fuel per kg

air, but a molar basis can also by used, kmol fuel per kmol air. The simplified combustion equation for a hydrocarbon fuel C_xH_y can be represented as

$$C_xH_y + a(O_2 + 3.76N_2) \rightarrow bCO_2 + cCO + dH_2O(g) + eH_2 + fO_2 + 3.76aN_2 . \quad (4)$$

For stoichiometric and fuel-lean conditions, $\phi \leq 1$, Equation (4) becomes

$$C_xH_y + a(O_2 + 3.76N_2) \rightarrow bCO_2 + dH_2O(g) + fO_2 + 3.76aN_2 , \quad (5)$$

while for fuel-rich conditions, $\phi > 1$, Equation (4) becomes

$$C_xH_y + a(O_2 + 3.76N_2) \rightarrow bCO_2 + cCO + dH_2O(g) + eH_2 + 3.76aN_2 , \quad (6)$$

where

$$a = \frac{x + \frac{y}{4}}{\phi} \quad (7)$$

Equations (4) through (6) are expressed for 1 kmol of fuel. Examining Equation (5) we see the coefficients for CO and H_2, products of incomplete combustion, are zero, since the equation represents the fuel-lean combustion case with excess air present to ensure complete combustion. The presence of O_2 as a product in Equation (5) further represents the excess air present in combustion of the fuel. Additionally, for the case of ϕ = 1, Equation (5) simplifies to stoichiometric combustion without O_2 present as a product. Similarly, the inclusion of CO and H_2 as products of incomplete combustion in Equation (6) demonstrates that fuel-rich combustion is represented, in which insufficient oxygen is present to drive the reaction to completion.

Since compression ignition engines, the subject of our study, operate with typical equivalence ratios of 0.8 (ϕ = 0.8), we will evaluate Equation (5). For $\phi \leq 1$, C, H, and O-atom balances on Equation (5) yield:

$$b = x \quad (8)$$

$$c = 0 \quad (9)$$

$$d = \frac{y}{2} \quad (10)$$

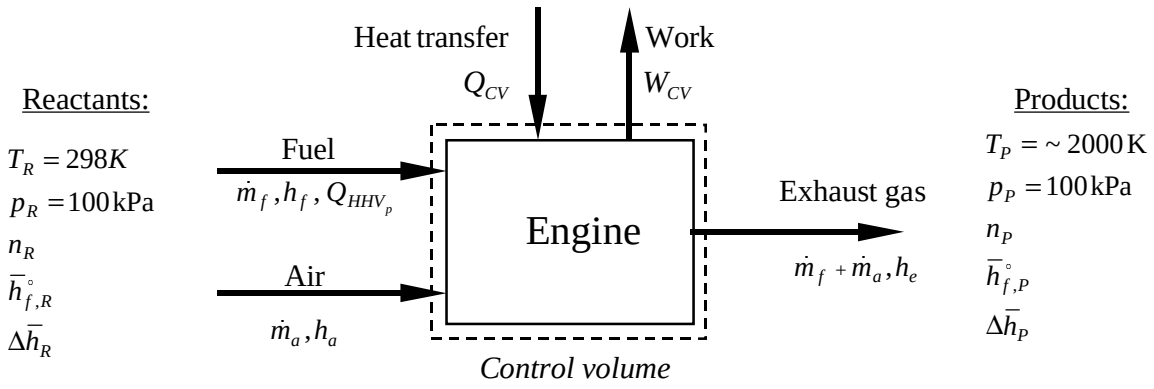

Figure 7: Simplified control volume around internal combustion engine

$$e = 0 \tag{11}$$

$$f = \left(\frac{1-\phi}{\phi}\right)\left(x + \frac{y}{4}\right) = (1-\phi)a \tag{12}$$

These coefficients are used to balance the combustion equation for a first law of thermodynamics analysis of the reacting combustion system.

First Law of Thermodynamics Analysis

A control volume is depicted around a combustion cylinder in Figure 7 for demonstration of a first law analysis. The first law of thermodynamics relates changes in internal energy on a control volume to heat and work interactions by the control volume with the environment. A first law analysis deals with end states only—chemical reactions or other changes in the species during reaction are not evaluated. For this reason, the zero internal energy, or enthalpy, reference state of species acting on the control volume must be at the same conditions. Temperature and pressure will define the reference state for the pseudo-constant pressure compression ignition process. Tabulated values of enthalpy for reactants and products will be used, and the combustion system's internal energy decreases because the process is exothermic.

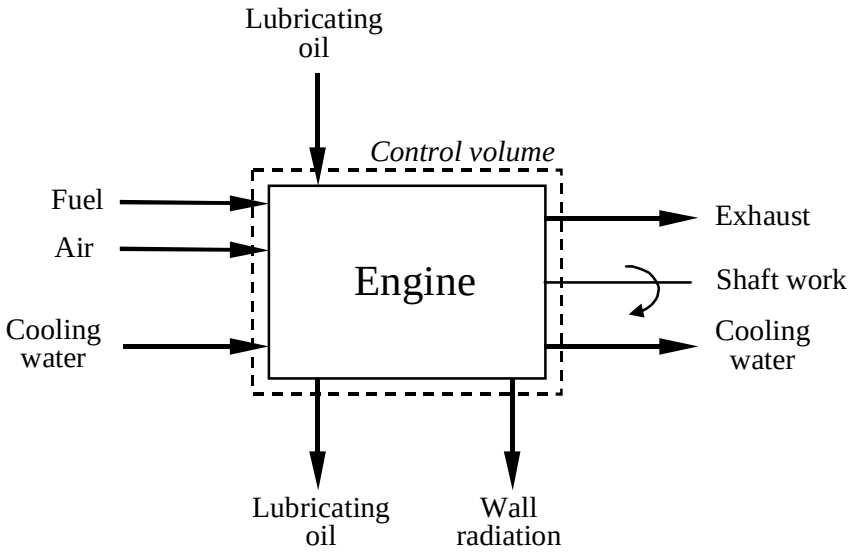

Figure 8: External control volume around ICE

Figure 7 shows fuel and air entering the control volume with enthalpies of h_f and h_a, and mass flow rates of $\dot{m}_f$ and $\dot{m}_a$, respectively. Exhaust gas leaves the control volume with enthalpy h_e and mass flow rate of $\dot{m}_f + \dot{m}_a$. Enthalpies of formation for reactants are balanced with the change in enthalpy of products in the form

$$Q_{CV} + \sum_R n_i \bar{h}_i = W_{CV} + \sum_P n_j \bar{h}_j \qquad (13)$$

where Q_{CV} is heat transfer from the control volume, W_{CV} is shaft or other work done by the control volume, and summations are of n moles and h enthalpies of reactants and products. Enthalpies are evaluated at reactant and product temperatures, T_R and T_P. Moles of reactant and product species, n_R and n_P, are described by the governing combustion equation, such as Equation (5). Equation (13) can be used to find the heat transfer from the control volume given the flame temperature, or the flame temperature can be estimated using an iterative process demonstrated in Chapter 5.

The control volume can be expanded to include losses from the internal combustion engine. Figure 8 depicts a control volume around an ICE including heat inputs and losses, and shaft work. The heat input to an ICE comes from the heat value of the fuel combusted, cooling water inlet temperature, and lubricating oil inlet temperature. Energy leaves the control volume of the ICE in the form of heated lubricating oil and cooling water, shaft work, exhaust gases, and radiative heat transfer to the crankcase and cylinder. Other losses can include incomplete combustion, blowdown, and pumping. Blowdown occurs during the heat addition process: as the fuel—air mixture ignites and begins expanding, gases can slip past the cylinder rings into the crankcase. Pumping losses are incurred through power used to pump the lubricating oil and cooling water. Heat transfer modes and effects in ICEs are discussed in the following sections.

Heat Transfer Effects in ICEs

Conduction, convection, and radiant heat transfer are significant to the design, operation, and

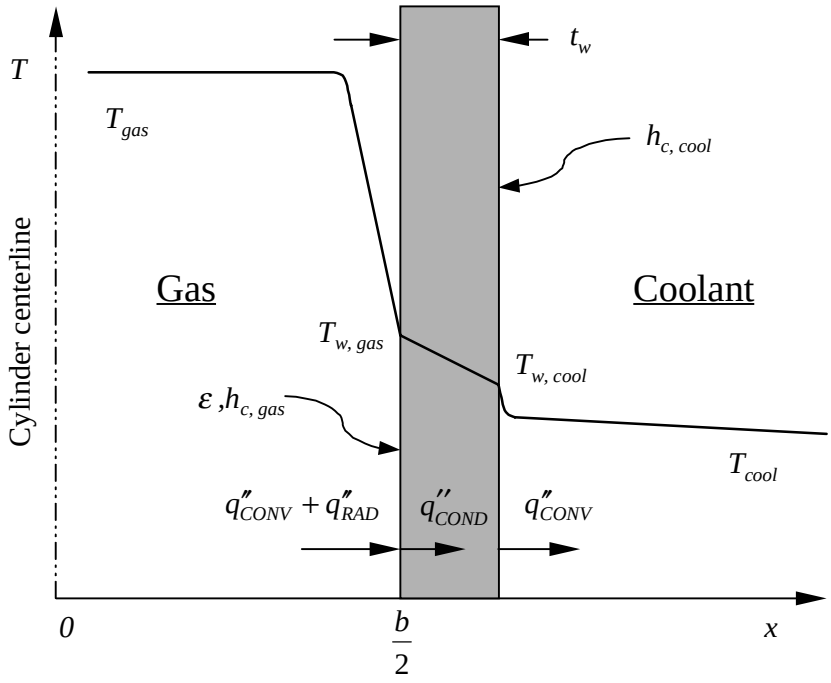

Figure 9: Heat transfer from combustion gas to coolant

evaluation of internal combustion engines. Figure 9 depicts the gas and coolant temperature versus distance from the combustion cylinder centerline in an ICE. Temperature, *T*, is plotted on the y-axis, which corresponds with the combustion cylinder centerline at $x = 0$. The temperature of the gas in the cylinder falls as it approaches the inner wall of the cylinder, at $\frac{b}{2}$, where *b* is the cylinder bore. Both convective heat flux, q''_{CONV}, and radiative heat flux, q''_{RAD}, occur between the combustion products and the inner cylinder wall. The gas-side convective heat transfer coefficient, $h_{c,gas}$, and the emissivity, ε, at the inner cylinder wall are needed to calculate q''_{CONV} and q''_{RAD}. Heat is then conducted through the cylinder wall, shown as q''_{COND}, with cylinder wall thickness t_w. Temperature through the cylinder wall is reduced from $T_{w,gas}$ on the gas side to $T_{w,cool}$ on the coolant side. Temperature drops through the thermal boundary layer on the coolant side near the cylinder wall, as governed by the convective heat transfer coefficient, $h_{c,cool}$, between the coolant and outer cylinder wall. The individual modes of heat transfer, governing equations, and relevant effects on ICEs are discussed below.

Conduction

Conduction heat transfer refers to the transfer of heat by molecular motion and interaction in solids and non-moving fluids. Heat flux (q'') is governed by the well-known Fourier's Law for steady heat conduction,

$$q''_{COND} = -k\nabla T \tag{14}$$

where *k* is the thermal conductivity, W/m·K, and ∇T is the gradient of temperature, defined as $\frac{\partial^2 T}{\partial x^2} + \frac{\partial^2 T}{\partial y^2} + \frac{\partial^2 T}{\partial z^2}$. In addition to conduction heat transfer through the cylinder wall, as shown in Figure 9, heat is also immediately conducted from the combustion gases through the piston, valves, and cylinder head.

Convection

Heat transfer by convection occurs between a fluid in motion relative to a fluid or solid surface. For steady flow-forced convection, or convection driven by forces other than gravity, the convective heat flux from a fluid at temperature T to a solid surface at T_w is given by

$$q''_{CONV} = h_c (T - T_w) \tag{15}$$

where h_c is the convective heat transfer coefficient, W/m^2·K. Actual flows in the combustion cylinder are turbulent and unsteady, and detailed analyses require the use of the conservation, momentum, and energy equations. Convection is the primary form of heat transfer in the ICE, and Table 3 summarizes the processes in which heat is transferred by convection from the combustion gases in an internal combustion engine.

Radiation

Radiation heat transfer occurs through the emission and absorption of electromagnetic waves in the visible (0.4 μm to 0.7 μm) and infrared (0.7 μm to 40 μm) range (Eckert and Drake, 1987). Although all substances radiate energy, it is only at elevated temperatures that the heat flux radiated becomes significant. This is demonstrated by the radiative heat flux equation

$$q''_{RAD} = \varepsilon \sigma (T_s^4 - T_{sur}^4) \tag{16}$$

Table 3: Summary of convection heat transfer in an ICE

Heat Source	Convective Heat Flux To:
Combustion gases (compression, expansion)	Cylinder heads, cylinder valves, cylinder walls, pistons, and O-rings
Outside cylinder walls, cylinder heads	Engine coolant
Piston, O-rings	Lubricant (or piston coolant, if present)
Combustion gases (exhaust)	Exhaust valves, exhaust ports, and exhaust manifold
Intake manifold	Intake air
Coolant	Radiator, environment

where ε is the emissivity of the surface, σ is the Stefan-Boltzmann constant, T_s is the maximum blackbody temperature of the surface, and T_{sur} is the temperature of the surrounding environment. Shape factors are applied to account for fractions of radiation from a source interacting with the recipient surface. In combustion engines the radiant heat sources are primarily particulate (soot), water vapor, and CO_2 (Zhou et al., 1987). This radiant heat falls on the cylinder walls, piston surface, and valve body.

ICE radiant heat transfer is difficult to estimate and measure. Radiant heat transfer is also more significant in diesel engines than spark ignition engines, due to higher soot content of the diesel combustion products. High-temperature intermediate soot particles and high flame temperatures are the source of radiant heat to the cylinder walls, piston, and combustion gases. The radiant heat transfer due to soot depends on the particle size distribution, number density, flame geometry, and, as shown in Equation (16), the soot temperature. Emissivity reportedly ranges from 0.8 to 0.9 during periods of peak radiation. The average radiant heat flux reportedly ranges from 5 to 50 percent of total heat flux, rising with increases in engine load (Kays, 1989).

The discussion here has focused on the heat transfer and thermodynamic effects of the combustion process, but engine materials require cooling, and the design of this cooling system is a significant aspect of overall ICE design. Kays (1989) evaluated the design of air and liquid cooling systems for ICEs according to fundamental heat exchanger principles. He demonstrated that engine head design, radiator manufacturing methods and costs, and coolant pumping losses often control radiator design, verses optimal waste heat exchange from the cylinder to the coolant.

Engine Variable Effects

The ICE is a thermodynamic heat engine, so any changes to components, parameters, or work per unit time will affect the heat flux through the engine to the environment. Table 4 summarizes how changes in important engine variables affect heat flux from the combustion gases.

Several trends listed in Table 4 are significant to the present study. Increasing the load or speed of an engine, thus increasing the power output, requires increasing the fuel/air mixture flow. With an increase in $\dot{m}_f$, the fuel flow rate, the heat transfer rate q'' through the engine is increased from the additional heat input. Conversely, reducing $\dot{m}_f$ will lower q''. This effect correlates to the present study when considering the $\dot{m}_f$ diesel fuel component of the diesel—water mixture is decreased when total $\dot{m}_f$ remains constant through the engine for a given load or speed. In other words, if the total fuel flow rate is not changed when adding water to the fuel, then the combustible fuel flow rate is reduced, lowering the heat transfer rate in the engine.

From the discussion of convection heat transfer and Equation (15), if the convective heat flux is

Table 4: Engine variable effects on heat flux

Variable	Direction	Effect	Discussion
Speed or load	↑	Greatest effect, increases heat flux, q''	Increases $\dot{m}_f$, fuel flow rate
Equivalence ratio, ϕ (AF/AF_s ratio)	↑	q'' increases to ϕ = 1.1, then decreases	Maximum thermodynamic gas temperature reached
Compression ratio, r_c	↑	Decreases q'' until $r_c \approx 10$, then q'' increases slightly	Lower expansion and exhaust temperatures
Injection timing (CI)	Delay	Decreases q''	Combustion occurs during larger cylinder volume, V_c
Spark timing (SI)	Delay	Decreases q''	Combustion occurs during larger cylinder volume, V_c
Swirl, mixing	↑	Increases q''	Gas velocities increased
Inlet temperature	↑	Increases q''	Linear increase in temperature throughout heat exchange processes
Coolant temperature	↑	May reduce q''	Increases component temperature
Cylinder wall thermal conductivity, k	↓	Decreases q''_{CN} through cylinder wall	May cause heat flux to combustion gases from wall, resulting in pre-ignition

lowered, then the temperature difference between the combustion gases and the cylinder wall will also be lowered. Given a constant convective heat transfer coefficient and constant coolant temperature, we can theorize that the flame temperature will be lower to result in this lower heat flux.

Reducing cylinder wall thermal conductivity *k* decreases the conductive heat transfer through the wall. This can result in a higher inner cylinder wall temperature and lead to pre-ignition of the fuel—air mixture. The effect is similar that of insulating the cylinder, which can improve compression ignition engine performance when properly designed (Heywood, 1988).

Efficiency and performance gains in ICEs have been significant, and combustion modifications and control devices have substantially reduced air pollutant emission rates. Modeling and experimental analysis of fuel spray, atomization, and vaporization has improved the understanding of the onset and progression of diffusion combustion in the diesel engine. Spray formation is increasingly important as advanced swirl designs are incorporated into the combustion chamber to improve mixing.

Researchers are also improving numerical flow simulation methods for internal combustion processes. Some models have been under development and refinement for nearly 30 years. Boundary value solutions to the differential equations using finite difference methods are valuable for general solutions. Finite element analysis offers a solution to correlate predicted and experimental results, because the three-dimensional physical constraints can be used as boundaries for the heat transfer and momentum equation solutions (Campbell, 1979).

Fuel ignition and resultant flame quenching is another area of focus in internal combustion engines. Research includes modeling and understanding the rates and patterns of fuel ignition, including the spray pattern effects, and the passive or active quenching of the flame. Active quenching of the flame is often accomplished by introducing water, alcohols, or other lower heating value additives to the fuel, which is the premise of the present research. Passive flame

quenching occurs at the engine combustion chamber walls. Flame quenching causes incomplete combustion and thus results in higher emissions of unburned hydrocarbons.

Improvements in measurement techniques are important to all aspects of ICE analysis. An experimental study of ICEs involves temperature measurements somewhere in the combustion process. As shown in the convective and radiant heat equations, Equations (15) and (16), the cylinder wall temperature, T_w, is fundamental to ICE heat transfer analysis. The high combustion temperatures can interfere with thermocouple signals, and the unsteady nature of the combustion field makes direct measurement of radiant flame temperature difficult. Spectroscopic techniques using optical fibers to transfer a flame image from the combustion chamber to a photoelectric transducer can be used to measure the spectral illuminance, which is then correlated to the flame temperature (Nagese and Funatsu, 1990).

CHAPTER 3

INTERNAL COMBUSTION ENGINE EMISSIONS

The review thus far has focused on the physical and thermodynamic properties of internal combustion engines. The chemical pathways of formation, mitigation methods, and engine factors affecting air pollutant emissions from ICEs are discussed in the present chapter. This review is important in predicting and evaluating how the ICE air pollutant emission levels respond to the alternative fuel.

Pollutant Formation

The air pollutant emissions from internal combustion engines vary with the operational and design parameters discussed earlier in Chapter 2. Other factors affecting air pollutant emissions include ignition and valve timing, fuel types and additives combusted, lubricants employed in the engine, and exhaust gas treatments employed (Abdel-Rahman, 1998). These air pollutant emissions can be broadly characterized as gaseous and non-gaseous emissions.

Gaseous Emissions

The major gaseous pollutants emitted include oxides of nitrogen (NO_x,) and carbon monoxide (CO). NO_x refers to mixtures of nitric oxide (NO) and nitrogen dioxide (NO_2). Small amounts of sulfur dioxide (SO_2), also a criteria pollutant regulated under the CAAA, are emitted. SO_2 emissions from ICEs are solely a result of fuel-bound sulfur and are readily reduced by limiting sulfur in the fuel.

Table 5: Relative levels of ICE air pollutant emissions

	Concentration	
Pollutant	ppm	g/kg fuel
NO_x	500-1000	20
CO	1000-2000	200
HC (as C_1)	3000	25

Non-Gaseous Emissions

The primary non-gaseous pollutants are unburned or partially burned hydrocarbons (HCs). Relative levels of both gaseous and non-gaseous emissions from ICEs are shown in Table 5. These are only ranges, since actual emissions vary greatly on engine design, fuels combusted, and combustion and post-combustion controls involved. HCs are divided into reactive and nonreactive categories, based upon their role in photochemical smog formation. The simplest such breakdown is categorizing HCs as methane and nonmethane hydrocarbons (NMHCs), since all HCs except for methane (CH_4) will react given sufficient time.

NO_x Formation

NO_x is referred to here as mixtures of nitric oxide (NO) and nitrogen dioxide (NO_2). NO_x emissions are controlled because NO and NO_2 contribute to the formation chemistry of low-level ozone, or smog, an environmental and human health hazard. NO_2 is also directly of concern as a human lung irritant.

NO_x can also be defined to include other oxides of nitrogen, including N_2O, NO_3, N_2O_4, and N_2O_5. These additional nitrogen oxide species are insignificant in the emissions from ICEs, and readily react to NO and NO_2. NO generally accounts for over 90 percent of the total NO_x emissions from fossil fuel combustion, with the remainder being NO_2. The formation of NO can be explained by three different mechanisms (Turns, 1996):

1. The Extended Zeldovich mechanism, or thermal NO, in which O, OH, and N_2 are in equilibrium concentrations
2. Other mechanisms with NO formation rates above that predicted by the Extended Zeldovich mechanism, including
    a. Fenimore CN and HCN pathways
    b. N_2O-intermediate route
    c. "Super-equilibrium" concentrations of O and OH in combination with the Extended Zeldovich mechanism
3. Fuel nitrogen mechanism, in which fuel-bound nitrogen is oxidized to NO.

The primary pathway for NO formation is oxidation of atmospheric molecular nitrogen (N_2) through the thermal or Zeldovich mechanism:

$$O + N_2 \Leftrightarrow NO + N \quad (17)$$

$$N + O_2 \Leftrightarrow NO + O \quad (18)$$

Extending the thermal NO formation mechanism to include the hydroxyl radical reaction with nitrogen was proposed by Lavoie et al (1970):

$$N + OH \Leftrightarrow NO + H \quad (19)$$

Thermal NO formation rate is slow relative to combustion and is considered unimportant below 1800 K. Thermal NO formation attributed to Equations (17) through (19) is considered formed in the post-combustion exhaust gases.

Prompt NO, also referred to as the Fenimore mechanism, is NO that is quickly formed in the premixed laminar flame before thermal NO has formed. Hydrocarbon radicals react with molecular nitrogen to create hydrogen cyanide as an intermediate to NO formation in the following steps:

$$CH + N_2 \Leftrightarrow HCN + N \quad (20)$$

$$HCN + O \Leftrightarrow NCO + H \quad (21)$$

$$NCO + H \Leftrightarrow NH + CO \quad (22)$$

$$NH + H \Leftrightarrow N + H_2 \quad (23)$$

$$N + OH \Leftrightarrow NO + H \quad (24)$$

Prompt NO formation is also considered insignificant in internal combustion engines due to the thin flame fronts, short residence times, and high pressures in the combustion chamber.

The formation of NO through an N_2O intermediate mechanism is important in fuel-lean (ϕ < 0.8), lower temperature conditions (T < 1800 K). The three steps are:

$$O + N_2 + M \Leftrightarrow N_2O + M \quad (25)$$

$$H + N_2O \Leftrightarrow NO + NH \quad (26)$$

$$O + N_2O \Leftrightarrow 2NO \quad (27)$$

The *M* in Equation (25) represents a third body collision molecule. The significance of the N_2O intermediate mechanism can be seen in Equation (27) where two moles of NO are formed per mole of N_2O. While our subject engine operates at ϕ = 0.8, the flame temperature is slightly higher than 1800 K, so N_2O intermediate pathway formation of NO is probably not significant.

Fuel-bound nitrogen is another source of combustion NO emissions. This process is significant in coal combustion, where bituminous coal contains up to 2% by mass bound nitrogen. Nitrogen in the fuel is quickly reacted to HCN or ammonia, NH_3, and follows the reaction steps beginning with Equation (21) for prompt NO formation. Kerosene and gasoline fuels contain trace to zero quantities of nitrogen, so fuel-bound nitrogen contribution to NO formation is not considered significant in internal combustion engines.

The final reaction mechanism considered here for NO_x formation is production of NO_2. Reactions contributing to the formation and destruction of NO_2 are as follows:

$$NO + HO_2 \Leftrightarrow NO_2 + OH \text{ (formation)} \quad (28)$$

$$NO_2 + H \Leftrightarrow NO + OH \text{ (destruction)} \quad (29)$$

$$NO_2 + O \Leftrightarrow NO + O_2 \text{ (destruction)} \quad (30)$$

The HO_2 radicals form in low-temperature regions, leading to NO_2 formation through Equation (28). NO_2 destruction via reaction with the H and O radicals are active at high temperatures [Equations (29) and (30)]. Thus NO formation from NO_2 would be preferred at high temperatures and NO_2 would only survive during low-temperature cooling of exhaust gases. This validates the previous statement that most of the NO_x emitted from internal combustion engines is NO.

Heywood (1988) reports the following relationship for NO formation rate based upon empirical data and the assumption of equilibrium concentrations of O, O_2, OH, H, and N_2, by decoupling the NO formation from combustion (i.e., assuming NO formation in post-combustion gases always dominates NO produced in the flame):

$$\frac{d[\mathrm{NO}]}{dt} = \frac{6\times10^{16}}{\sqrt{T}}\, \mathrm{e}^{\left(\frac{-69{,}090}{T}\right)} [\mathrm{N}_2]_\mathrm{e} \sqrt{[\mathrm{O}_2]_\mathrm{e}} \qquad (31)$$

where $[\ ]_e$ denotes equilibrium concentrations. The significant dependence of temperature on NO formation rate in Equation (31) is evident. Equation (31) will be used later in Chapter 5 to calculate the relative NO formation rate from estimated flame temperature changes for comparison with measured percent NO reductions.

CO Formation

Carbon monoxide (CO) emissions from ICEs are a concern from toxicological effects on humans.. The formation of CO from the combustion of the hydrocarbon radical, *R*, is as follows:

$$\mathrm{RH} \rightarrow \mathrm{R} \rightarrow \mathrm{RO2} \rightarrow \mathrm{RCHO} \rightarrow \mathrm{RCO} \rightarrow \mathrm{CO} \qquad (32)$$

Once formed, CO is slow to oxidize to CO_2, with water providing the primary oxidant source through the following steps:

$$\mathrm{CO} + \mathrm{O}_2 \rightarrow \mathrm{CO}_2 + \mathrm{O} \qquad (33)$$

$$\mathrm{O} + \mathrm{H}_2\mathrm{O} \rightarrow 2\mathrm{OH} \qquad (34)$$

$$\mathrm{CO} + \mathrm{OH} \rightarrow \mathrm{CO}_2 + \mathrm{H} \qquad (35)$$

$$H + O_2 \rightarrow OH + O \quad (36)$$

The reaction in Equation (33) is slow, with primary oxidation of CO occurring through Equation (35), with Equation (36) producing OH radicals feeding back to Equation (35). Diatomic hydrogen (H_2) can also provide oxidation of CO through formation of HO_2, but H_2 is not formed in sufficient quantities in ICE combustion to contribute to CO oxidation.

Control Technologies

Technologies to control air pollutant emissions from ICEs can be categorized as process or post-combustion controls. Process controls include changes and improvements to the combustion chamber, fuel/air delivery, and engine components aimed at reducing air pollutant emissions. For example, CFD analysis and design has been used to improve and air intake valve ports to enhance fuel—air mixing. Post-combustion controls include catalytic converters and other technologies applied to react with combustion exhaust constituents including NO_x, CO, HCs, and particulate.

Combustion Modifications

Exhaust gas recirculation (EGR) is commonly employed to reburn combustion by-products, especially CO and particulate. EGR also dilutes the intake air oxygen concentration, increasing the heat capacity of the combustion products per unit of heat release, lowering the combustion flame temperature (Turns, 1996). Larsen et al. (1996) reported 50% NO_x reduction at 20% EGR, but CO emissions doubled and fuel economy decreased 8%. Exhaust gas recirculated on diesel engines must be well-filtered to prevent fuel sulfur and exhaust particulate from eroding and corroding engine intake valves, cylinders, and pistons.

Adjusting fuel injection timing is an effective method for decreasing NO_x emissions. Traditional practice is to delay fuel injection into the combustion chamber to lower the final flame temperature, but this generally results in higher unburned hydrocarbon emissions. Yanagihara (1997) demonstrated reduced NO_x production by shortening the injection duration

while advancing the fuel injection. His results are attributed to improved fuel—air mixing prior to combustion, which both improves combustion efficiency and reduces unburned hydrocarbons.

Selective and Non-Selective Catalytic Reduction

Selective catalytic reduction (SCR) involves the use of a catalyst generally requiring an additive, such as ammonia, to initiate NO_x reduction chemistry. A common application of SCR in internal combustion engines is the Pt, Rh, and Pd three-way catalytic converters used on spark ignition engines combusting gasoline. Unburned hydrocarbons act as the selective reducing agent for the catalysts. Non-selective catalytic reduction (NSCR) also involves the use of a catalyst but without the need for an additive to reduce NO_x. The application of SCR or NSCR catalysts in a diesel exhaust is severely complicated (1) primarily by the higher excess oxygen content of diesel exhaust, resulting in a net oxidizing environment, and (2) by the presence of sulfur in diesel fuel and resulting catalyst poisoning by sulfur dioxide in the exhaust gases. Significant research is ongoing using secondary injection of small quantities of fuel in the exhaust stream to act as the reducing agent, with demonstrated NO_x reductions of approximately 45 percent at reasonable space velocities and high fuel metering rates (Nakatsuji et al., 1998).

Water Injection

Four major approaches for introducing water into the combustion zone have been reported in the literature:

1. Fumigating the water into the engine intake air
2. Direct injection into the engine through separate injectors
3. In-line mixing of water and fuel prior to injection (unstabilized emulsion)
4. Mixtures of stabilized emulsions treatable as a single-phase drop-in replacement fuel

Urbach et al. (1997) demonstrates water mist injection into the bell housing of diesel-fueled turbine engines with promising results. Water mist introduced to the intake of reciprocating compression ignition ICEs, particularly two-stroke engines with the intake air passing through the

crankcase, poses significant corrosion potential. Separate water injecting valves in the engine avoids intake system contact with the mist (Yoshihara et al., 1996). Several authors have evaluated all or most of the options for introducing water into the combustion process and have primarily determined that water-in-fuel emulsions, stabilized or unstabilized, are most effective in reducing NO_x, BSFC, and result in lower increases of CO and UHC emissions (O'Neal et al., 1981; Greeves et al., 1976).

An emulsion is defined as a mixture of two or more generally insoluble liquids. A permanent emulsion exists when sufficient droplet sizes have been reached to prevent the separation of the insoluble materials. Unstabilized emulsions are generated through the high-speed, high-shearing of particles and solids in a liquid. A limiting concern with emulsions is the high capital costs of emulsification mixers and pumps, which are used extensively in the food and agriculture industries.

Unstabilized emulsions require high shear to suspend small droplets of water in the fuel (Greeves et al., 1976). An advantage of unstabilized emulsions are reduced fuel costs, due to lack of additives needed, and reduced emissions from not combusting surfactants or other emulsifying agents (De Vita, 1989). Ulrich and Kessler (1992) propose a complex fueling system including a vortex chamber to provide in-line mixing of water and diesel fuel without requiring the addition of an emulsifying agent. Diesel fuel pumps, including the unit on our Detroit Diesel 4-71 engine, operate at high volume and high pressure, with a recirculation loop back to the fuel tank. This serves several purposes:

1. A high-volume pump can create the high-pressure needed for the fuel injectors at less expense
2. Recirculating warms the fuel and helps resist gelling at low temperatures
3. The warmed fuel improves combustion

All of these factors contribute to the effectiveness of an in-line fuel—water emulsifying system, assuming that retrofitting the fuel system is acceptable.

Stabilized emulsions use an emulsifying agent to suspend the water in the fuel and reduce the energy required for a permanent emulsion. The Air Force preferred a drop-in replacement fuel, without the requirement for modifying the engines or fueling system. The current research thus uses a surfactant to create a permanent, stabilized emulsion that can be treated as a single-phase fuel.

A drawback to water—fuel emulsions is the amount of air bubbles reportedly contained in the emulsion mixture. Sawa and Kajitani (1992) evaluated the effect of water—fuel emulsions on diesel engine performance and emissions under transient conditions. They conclude that air bubbles in the fuel and its variability contributes to fluctuation in the injection timing and a poorer performance under transient conditions. They recommend removal of bubbles from the water—fuel emulsion.

Research has also been conducted extensively on the use of additives to improve the lubrication, reduce the corrosive effect of water in the fuel, and improve the emulsion stability. Nitrate-containing ignition improvers are recommended to reduce exhaust emissions (Schwab, 1997). Lubricity additives composed of dimer or trimer acides, phosphate esters, sulfurized castor oils are recommended by Peter-Hoblyn et al. (1998), and catalysts can also be used in situ in the fuel to reduce NO_x (Peter-Hoblyn et al., 1996). In addition to providing lubrication improvement, additives to water—fuel emulsions can be employed for antifreeze characteristics (Marelli, 1995), obviously important when significant volume percents of water are present in a fueling system in freezing climates. Montagne et al. (1987) demonstrated that surfactants added to diesel fuels can both clean up fuel injectors and prevent further injector deposits. They also reported a slight increase in NO_x from the combustion of the surfactants, as we will experience without also adding water to the fuel.

Crookes et al. (1990) attributes water—fuel emulsions with improved combustion and lower particulate and NO_x emissions to the secondary atomization of the water, often designated as microexplosions. Yoshimoto et al. (1989) extensively examined the microexplosions of

emulsified fuels and determined that there is a minimum percent water content in the emulsion required for microexplosions to occur, and that the percent increases with the kinematic viscosity of the fuel.

Table 6 provides a summary of water injection and water-in-fuel emulsion research in the literature related to the present study. Note that Montagne et al. (1987) reported a 5 percent NO_x *increase* when adding surfactants only to diesel fuel for cleaning fuel injectors. This would lead us to eliminate the possibility that surfactants may solely contribute to the reduction of NO_x in our study. Crookes et al. (1990) were comparing diesel and vegetable oil fuels, both dry and as an emulsion with 10% water, by volume. Their results were included to demonstrate that small ratios of water provide negligible reductions in NO_x emissions. Small quantities of water are effective in improving BSFC, which could have merit for fuel savings. O'Neal et al. (1981) tested macro- and micro-emulsions to determine if water droplet size has a significant effect on NO_x reduction, BSFC, and other combustion parameters. They define micro-emulsion as

Table 6: Summary of diesel engine NO_x reduction using water and other additives

Reference	Method	Water, vol %	ΔNO_x, -%
Afify, 1985	Stabilized	45	83.3
Afify et al., 1987	Stabilized	40	65
Andrews et al., 1989	Stabilized	25	70
Crookes et al., 1990	Unstabilized	10	4
Fujita et al., 1987	Stabilized	30	65
Greeves et al., 1976	Unstabilized	80	60
Hsu, 1986	Stabilized	30	22
Montagne et al., 1987	Surfactant only		-5
Murayama et al., 1978	Stabilized	50	45
O'Neal et al., 1981	Macro-emulsion	20	25
	Micro-emulsion	20	23
Sawa and Kajitani, 1992	Stabilized	40	64
Valdmanis and Wulfhorst, 1970	Stabilized	50	72
Vichnievsky, 1975	Stabilized	55	59

emulsions with water droplet sizes smaller than the wavelength of visible light, approximately 555 nm, whereas macro-emulsions are characterized with water droplet sizes larger than the wavelength of visible light. Thus, micro-emulsions are reported to visually appear clear, while macro-emulsions appear cloudy. Our fuel mixture would be characterized in this manner as a macro-emulsion. As shown in Table 6, the reported NO_x reductions were 25 and 23 percent for macro- and micro-emulsions, respectively. They reported significantly-higher (unspecified) ratios of surfactant were required to establish a micro-emulsion, although they reported longer stability lifetime for the micro-emulsion. From our experience and the reports of O'Neal et al. (1981) we feel justified in using the minimum surfactant required to establish a stable macro-emulsion.

The data from Table 6 are plotted in Figure 10, except for that of Montagne et al. (1987). A

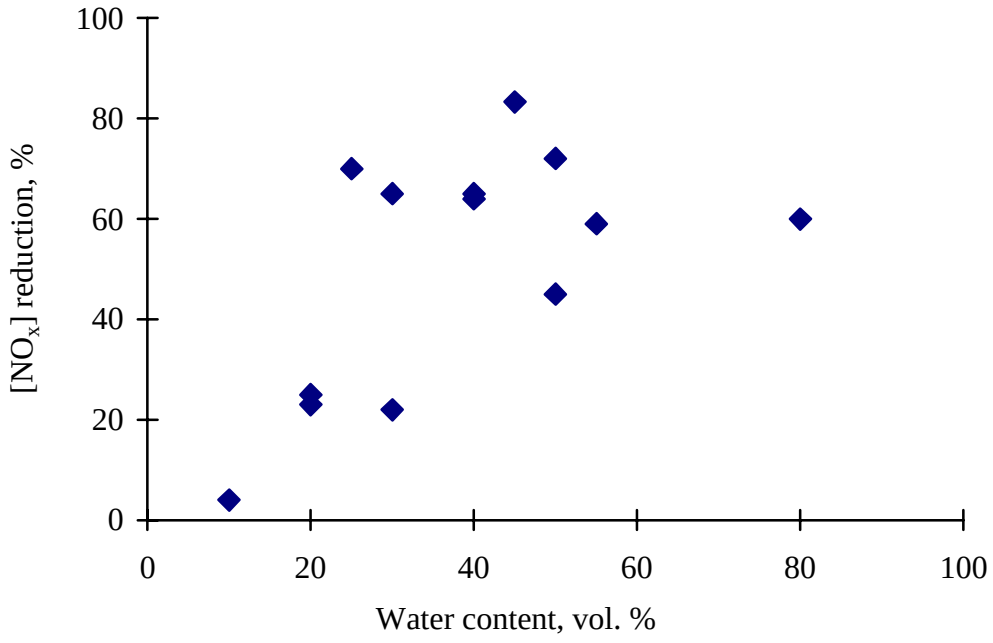

Figure 10: NO_x reduction as a function of fuel—water emulsion water content reported in the literature

trend is visible for reduced NO_x emissions with increased water content in the fuel. As shown in Table 6, this data represents 11 independent research programs conducted across a span of 22 years.

Other Control Technologies

Canfield et al. (1997) described a filter cart designed for capture of NO_x, CO, VOCs, and particulate from the A/M32A-86 diesel generator. The device is a series of sub-systems, including a vermiculite filter to capture particulate, air-to-air heat exchanger and demister for cooling and dewatering, and granular activated carbon (GAC) filters to adsorb NO_x, CO, and VOCs. The filter cart is shown on the right of Figure 11, attached to an A/M32A-86. This device requires a large footprint.

After the GAC filters are saturated and adsorption rates begin to decline, the filters are thermally regenerated. Adsorbed gases are desorbed, and can either be compressed, bottled, and reused, or destroyed on-line via selective catalytic reduction. The vermiculite particulate filters are replaced and discarded after excessive increase in pressure drop. The filter cart requires a

Figure 11: NO_x filter cart for diesel exhaust capture

large footprint and would not be feasible to mobilize to a war-fighting theatre. Advantages include that one filter cart can service multiple generators, depending on the capacity of the filter cart, and it can be used to control emissions from other combustion sources.

Nonthermal plasmas have also been applied to diesel exhaust, and specifically applied to reduce NO_x emissions from the A/M32A-86 (Ackridge et al., 1997; Rolader et al., 1997; Federle et al., 1998). This application also required the use of a series of subsystems, including a ceramic particulate filter, nonthermal plasma discharge (NTPD) reactor tube with alcohol injection, and a wet gas scrubber. The particulate filter captures particulate and would be cleaned in-line using the hot exhaust gases. The NTPD essentially uses high-voltage, low amperage, high-pulse rate electrical discharges to generate reactive, oxidative species in the exhaust gases. The addition of alcohols is reported to increase the reaction efficiency, lowering electron volts required to oxidize NO to NO_2. The wet scrubber is then used to adsorb and react the NO_2 with water to form nitric acid, HNO_3, and then with sodium hydroxide, NaOH, to form sodium nitrate, $NaNO_3$, useful as a fertilizer. This system would also require a large footprint.

CHAPTER 4

EXPERIMENTAL METHODS AND PROCEDURES

A/M32A-86 Parameters

The diesel engine used in the study is a Detroit Diesel 4-71N 2-stroke diesel engine with forced induction. Engine data are presented in Table 7 and a schematic of the generator is shown in Figure 12. The manufacturer engine designation corresponds to a 4-cylinder engine with 71 in^3 (1163.5 cm^3) per cylinder.

The A/M32A-86 generator was originally supplied with the N65 fuel injector, having an orifice diameter of 1.651 mm (0.065 in) and a recommended injection timing setting of 3.708 cm

Table 7: A/M32A-86 parameters (from SM-ALC/TISEA, 1986)

Engine Model	Detroit Diesel 4-71N
Combustion chamber type	Direct injection
Number of cylinders	4
Displacement, cm^3	4,653.9 (284 in^3)
Bore, mm	107.95 (4.25 in)
Stroke, mm	127 (5 in)
Compression ratio	18.71 : 1
Rated power at 2100 rpm, kW	110.4
Power factor	0.8
Maximum electric power output, kW	72
Air box pressure, kPa abs.	34.1 (10.1 in Hg)
Air inlet restriction, kPa abs.	2.86 (11.5 in H_2O)
Exhaust back-pressure, kPa gauge	13.5 (4.0 in Hg)
Compression pressure, kPa gauge	3,900 (565 psi)

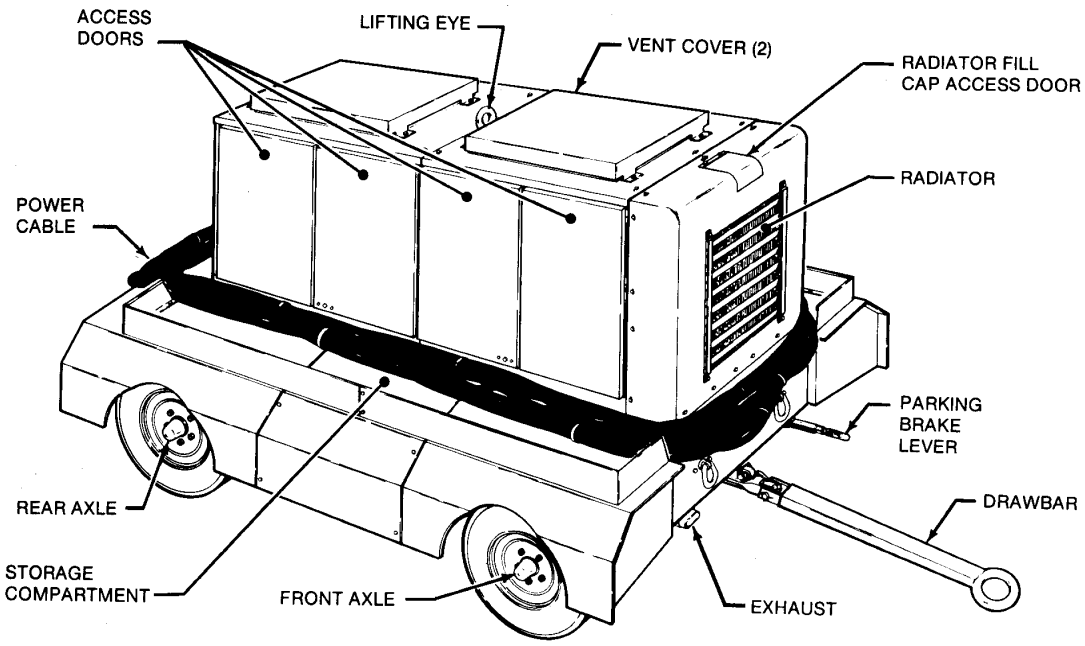

Figure 12: A/M32A-86 diesel generator (from SM-ALC/TISEA, 1986)

(1.460 in). This corresponds to the height of the piston from BDC when the fuel is injected. A larger dimension for fuel injection delay setting corresponds to a longer time delay before fuel injection. The dimensions are The N65 injector historically has a problem with plugging and fouling at low load levels. Thus, scheduled maintenance includes running the engine with generator at full load (72 kW) once a month to "clean out" the injectors. This results in significant NO_x and hydrocarbon emissions in a short period of time. Experimental results will be presented for both the N65 and N90 injectors. The N90 injector, with an orifice size of 2.286 mm (0.090 in.) was tested to increase the fuel flow rate delivered to the engine with the diesel—water emulsion.

Fuel Properties

Military specification (MIL-SPEC) diesel fuel was primarily used in the test, with properties shown in Table 8. We also conducted tests using JP-8, MIL-SPEC jet fuel. JP-8 is used in mobility applications of the generators. The Air Force has since standardized to the use of JP-8 in diesel engines to reduce the need to manage and maintain two fuel types and fueling systems. However, military specification diesel was in widespread use during the period of this test, and was therefore the focus of this study. Future project plans are discussed in Chapter 5 that include long-term testing of a fuel—water emulsion using JP-8.

The diesel—water fuel composition used in these tests is listed in Table 9. Experimental

Table 8: Common values for military diesel (from Avallone and Bauemeister, 1996, and U.S. DoD, 1995)

Property	Diesel MIL-F-16884J
Density @ 15°C, kg/m^3	876
API gravity, deg	40
Total sulfur, percent	0.5
Boiling point, °C	357
Endpoint, °C	385
Flash point, °C	60
Pour point, °C	-6
Hydrogen, wt %	12.5
Cetane number:	
Min	42
Max	43
Acid number, mg KOH/100 ml	0.3
Kinematic viscosity, cSt, @ 37.8°C:	
Min	1.7
Max	4.3
Specific gravity	0.889
High heating value, Q_{HHV_V}, kJ/kg	45,978
Low heating value, Q_{LHV_p} kJ/kg	41,425

results shown later indicating baseline exhaust temperature, [NO_x], and [CO] correspond to the standard fuel (diesel or JP-8) without water or additives. A corrosion inhibitor was selected to help offset potential corrosive effects of the water in the fuel during idle storage in the fuel tank. Lebedev and Nosov (1980) reported reduced wear on the upper area of the cylinder and piston (near TDC) in a Caterpillar 3304 engine with fuel—water emulsions, but also reported increased wear in the lower regions of the cylinder liner. They attribute the increased wear to sulfur in the diesel fuel blends. MIL-SPEC diesel and JP-8 traditionally contain little to no fuel-bound sulfur. For this study we were concerned with the perception of water in fuel as "corrosive," particularly to the fueling system, and included the corrosion inhibitor as a precaution. As discussed in Chapter 3, the emulsion improver allows a permanent emulsion to be stabilized more readily. Both additives are expected to reduce injector plugging, engine wear, and corrosion (Herbstman and Virk, 1989, Estefan and Brown, 1990, and Liu et al., 1993). Post-testing materials evaluations of the effect of the fuel—water emulsion on engine components would be valuable in determining and quantifying the necessity for a corrosion inhibitor. Eliminating the corrosion inhibitor would obviously lower the cost of the alternative fuel mixture. Intensive exhaust characterization using GC/MS would also be important to demonstrate that components of the corrosion inhibitor are not emitted from the engine. The corrosion inhibitor contains xylene and ethylbenzene, both targeted as potential carcinogens and targeted for extremely strict controls on their release from diesel and gasoline engines.

Table 9: Diesel—water emulsion properties

Fuel component	Percent, by volume
Water	30-45
Corrosion inhibitor	0.6
Emulsion improver (surfactant)	0.4
MIL-SPEC diesel	69-54

Sampling Procedure

NO_x emissions were measured using an Energy Efficiency Systems, Inc. ENERAC 3000 multigas analyzer with electrochemical cells measuring NO, NO_2, CO, O_2, SO_2, and percent HCs. The ENERAC 3000 meets the requirements and specifications of the U.S EPA's conditional reference method (U.S. EPA, 1995). The specifications and parameters for the ENERAC 3000 are listed in Table 10. The NO, NO_2, and CO sensors relied upon for this study are listed with an accuracy of ± 2.0%. As shown in Table 10, the ENERAC 3000 has three ranges for NO, CO, and SO_2. The unit is able to maintain a 1 ppm resolution across these broad ranges by including distinct electrochemical cells dedicated to the respective ranges. Systems that use a dilution factor will lose either accuracy or resolution when scaling to higher ranges. The calibration procedure for the ENERAC 3000 follows the EPA conditional test method and was performed prior to testing and data collection. The ENERAC 3000 includes a heated sampling probe with desiccant to absorb moisture in the exhaust to prevent damaging the electrochemical sensors.

An Omega thermocouple and digital thermometer were used to measure exhaust gas temperatures, traceable to National Institute of Standards and Testing (NIST) calibration standards. A fast-response thermocouple was used. A Fisher Instruments thermometer—hygrometer was used to read ambient relative humidity and dew point.

The A/M32A-86 is governed to 2100 rpm when under load. Load power settings listed are applied by a load bank, shown in Figure 13, used for engine routine maintenance. The load bank is an array of resistors that can be configured to mimic the varying loads of electric current drawn by an aircraft connected to the generator. Resistors are applied in three phases in 0-3 (variable)-, 3-, 6.5-, and 13-amp increments, with power measured on each phase with an analog meter. Total power is the sum of all three phases.

Water—fuel emulsion mixtures were hand-prepared in the laboratory in batch. An industrial high-speed clarifier was used to blend the water, fuel, and additives in desired concentrations. As mentioned in the Preface, a patent application is under review on the additive package, preventing further disclosure of the constituents. The goal of the additive package, in maintaining a stable

Table 10: ENERAC 3000 specifications (from Energy Efficiency Systems, Inc., 1995)

Measured parameter	Range	Resolution	Uncertainty, ±%
O_2	0–25.0%	0.1 %	0.2
NO	0-300 ppm	1 ppm	2
	0-1000 ppm	1 ppm	2
	0-3500 ppm	1 ppm	2
NO_2	0-500 ppm	1 ppm	2
CO	0-500 ppm	1 ppm	2
	0-2000 ppm	1 ppm	2
	0-20000 ppm	1 ppm	2
SO_2	0-500 ppm	1 ppm	2
	0-2000 ppm	1 ppm	2
	0-7000 ppm	1 ppm	2
HC (as CH_4)	0-6.00%	0.01%	10

Figure 13: Load bank for adjusting power load on generator

mixture, is to provide practical application of the water-in-fuel emulsion. Our results showed similar NO_x reductions to unstabilized emulsions, as also reported in the literature (Coon, 1981;Valdmanis and Wulforst, 1970; Sawa and Shuichi, 1992).

Data Collection

Results reported in the following figures and discussion are the averaged values of three sample points per indicated value. The NO_x, CO, and exhaust temperature readings were taken several minutes apart, tabulated, and averaged. The data are reported in X-Y scatter as functions of power load setting, in kW, on the generator.

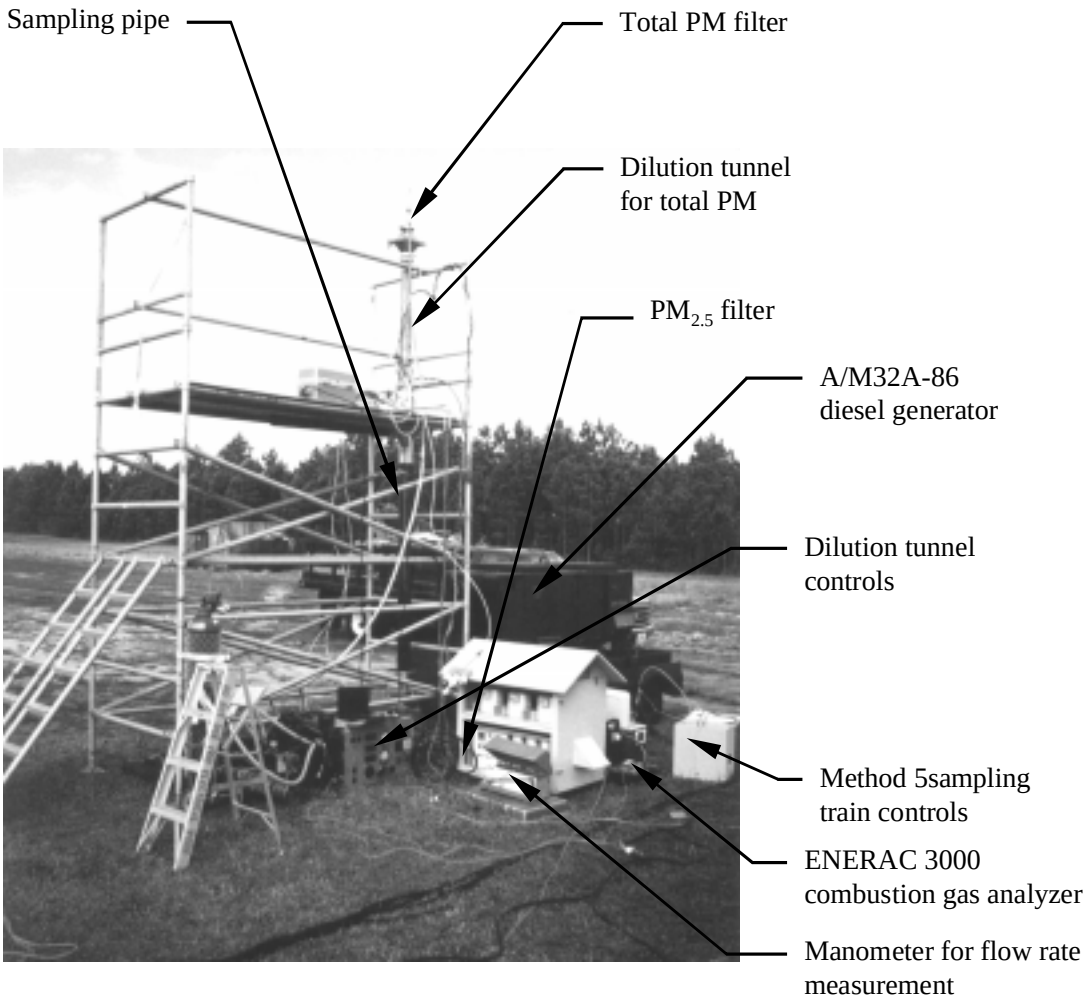

Figure 14: Exhaust gas sampling setup

The sampling system used in recent tests is shown in Figure 14. The diesel generator is visible in the rear behind the scaffolding. On top of the scaffolding is the dilution tunnel system used for capturing total particulate, and the "doghouse" structure houses pumps for filters to capture particulate fractions less than 2.5 μm. In front of the doghouse is a manometer to measure the pressure-drop of a static-pressure pitot tube, to calculate exhaust flow rate. A Z-shaped exhaust pipe is supported inside the scaffolding, from which all the exhaust samples are measured. To the right of the doghouse is a box housing a pump system for an EPA Method 5 sampling train to measure water content of the exhaust. The ENERAC 3000 used to measure

NO_x and CO is slightly visible to the immediate right of the doghouse. Attached to the left of the scaffolding is a helium tank for a portable GC/MS (Viking Instruments) used to characterize VOCs and SVOCs (not shown in the picture).

The ENERAC 3000 and Omega thermocouple were inserted through holes in the Z-shaped exhaust pipe immediately after the diesel generator exhaust pipe. The dilution tunnel sampling system requires a straight vertical run with 8 diameters of pipe length after the bend, which in turn required the construction of the Z-shaped exhaust extension and scaffolding support. The $PM_{2.5}$ filters feed off the flow through the dilution tunnel, which captures total particulate. Finally, the pitot tube for calculating exhaust gas flow rate is inserted in the upper horizontal run after the dilution tunnel.

CHAPTER 5

RESULTS AND DISCUSSION

Experimental Results

Experimental results are given in Figure 15 through Figure 21, where data are graphed for the NO_x and CO concentrations and exhaust temperature, T_e, as functions of power load on the generator. Power load is graphed, with the exception of Figure 19, from idle to 80 kW. Recall full electric load on the generator is 72 kW with diesel or JP-8 fuel. The idle condition is given an arbitrary value left of zero. Latter graphs are interpretations of the experimental data used to demonstrate the correlation between exhaust gas temperature, power setting, injector size, fuel water content, and exhaust gas composition.

Baseline Emissions

Figure 15 shows the NO_x, CO, and exhaust temperature for the diesel engine combusting diesel fuel, with the N65 and N90 injectors at various injection timing delay settings. Significant reductions in NO_x emissions are shown simply delaying the fuel injection for both injectors, with the N90 injector displaying significantly lower NO_x emissions. In fact, the Air Force is considering replacing the N65 stock injector with newer swirl injectors, based upon these and similar emission testing results elsewhere.

Comparing the NO_x and CO graphs in Figure 15, we see the customary tradeoff of higher CO emissions when NO_x is reduced. Note the N90 injector at 3.861 cm displays both the lowest NO_x and highest CO emissions. This is due primarily to the effect of fuel quenching causing

incomplete combustion and increased HC emissions, including CO. These results are consistent with trends described in the literature (Borman and Brown, 1992).

N65 Injectors

Figure 16 presents results with the N65 injector at 3.769 cm using the diesel—water emulsion. Note in Figure 16 the significant reductions in NO_x emissions using 30 and 43% water. Data for 30 and 43% water are not shown out to 72 kW because the generator could not develop that power output with the corresponding levels of water in the fuel. Exhaust temperature is a factor of 1.088 lower at 50 kW for the 30% diesel—water blend versus the standard diesel. This may be significant because the NO_x emissions were 1.75 times lower for the same range. From this, we can hypothesize that the relationship between NO_x and flame temperature is either nonlinear or chemical kinetic effects are responsible for the greater reduction in NO_x. Recalling the equilibrium NO formation rate, Equation (31), we would expect a nonlinear relationship between NO and temperature. Substituting $T_1 = 2000\,\mathrm{K}$ and $T_2 = \frac{2000}{1.088} = 1838\,\mathrm{K}$ into Equation (31), one obtains $\frac{d[\mathrm{NO}]_1}{dt} = 2.01\,\frac{d[\mathrm{NO}]_2}{dt}$, or that the rate of NO production should double with only a 1.088 factor increase in flame temperature, assuming exhaust gas composition is in equilibrium. Our data deviates from this estimate, since the slope $\left(\frac{d[\mathrm{NO}]}{dP}\right)$ of the baseline NO_x curve is only 1.53 times the slope of the 30% water curve. A likely source of the discrepancy is our use of exhaust temperature, versus in-cylinder flame temperature measurements. The excess water may continue to cool down the exhaust gases, giving a greater temperature difference between the baseline and 30% water than the NO_x levels would suggest. In other words, the flame temperature change is likely to be less than the exhaust temperature change.

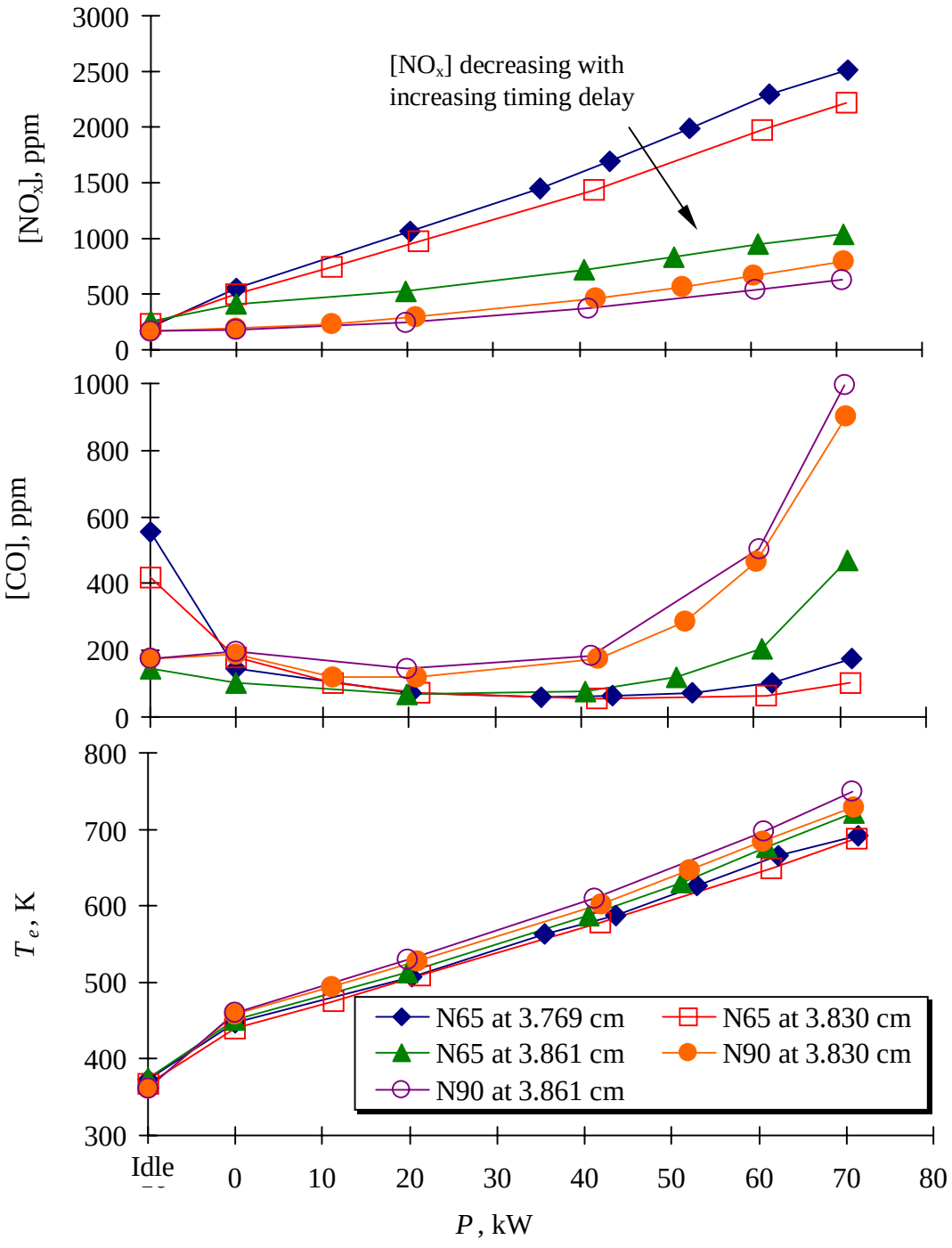

Figure 15: Baseline exhaust properties

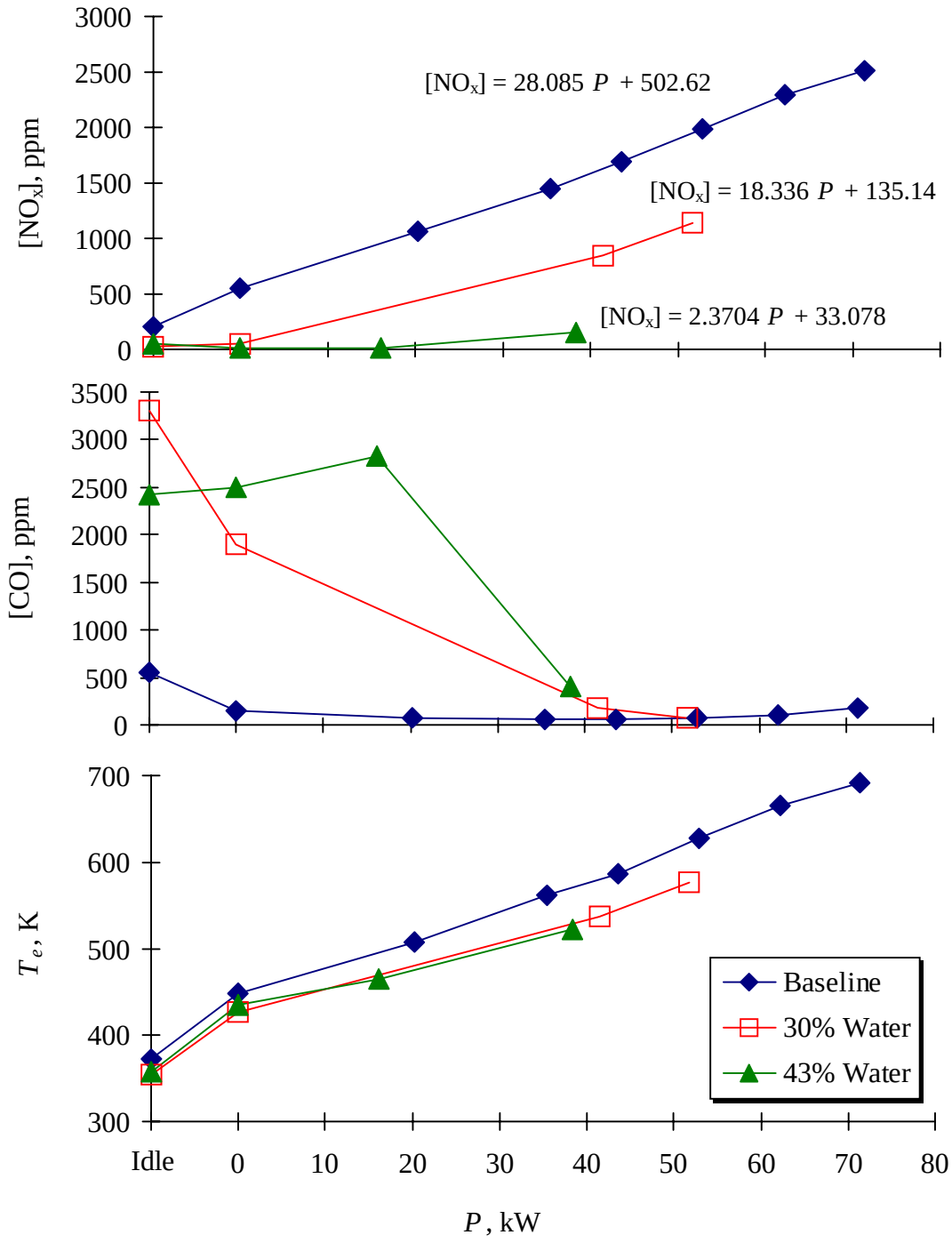

Figure 16: Exhaust properties with N65 injectors at 3.769 cm

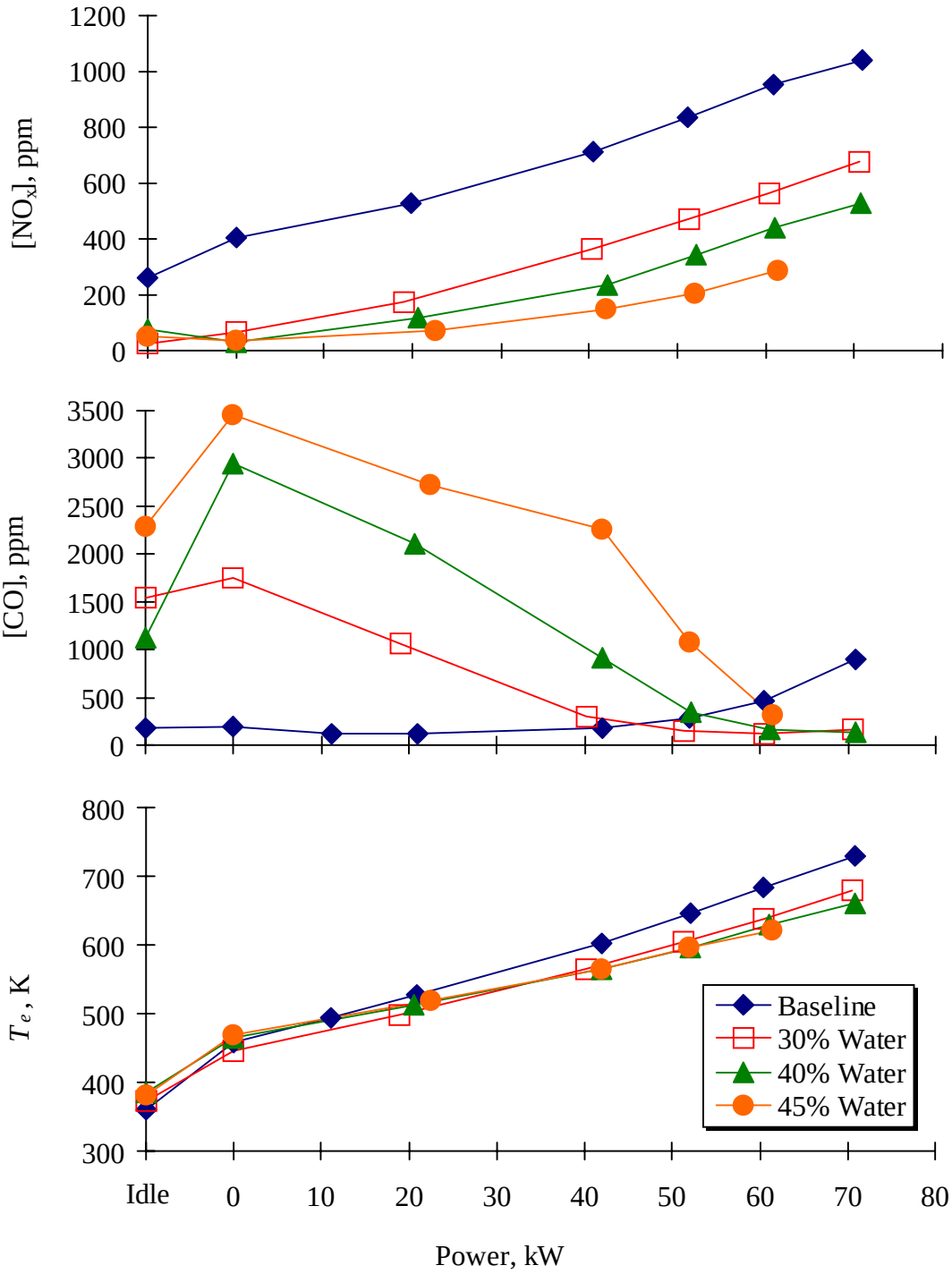

Figure 17: Exhaust properties with N90 injectors at 3.830 cm

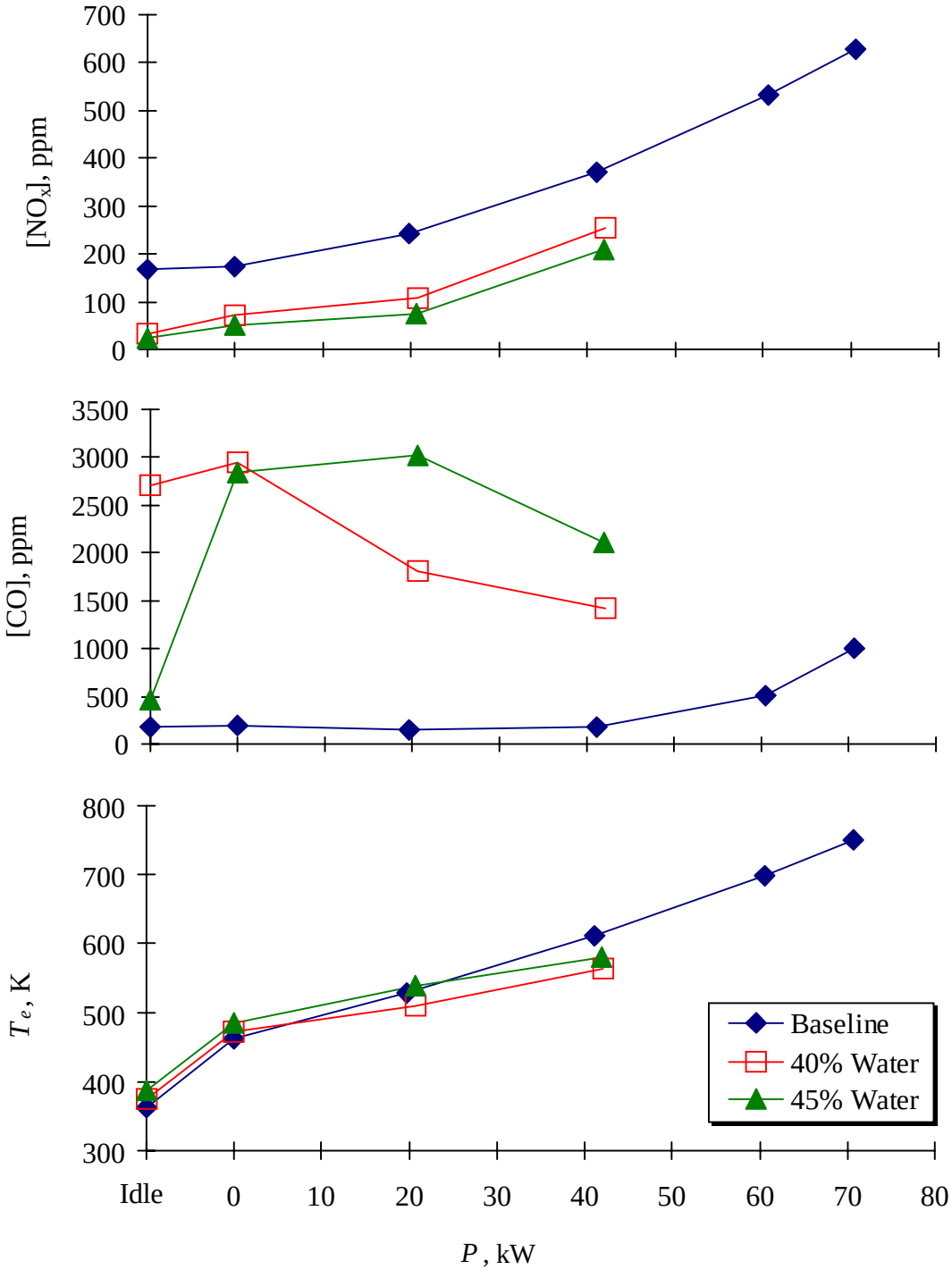

Figure 18: Exhaust properties with N90 injectors at 3.861 cm

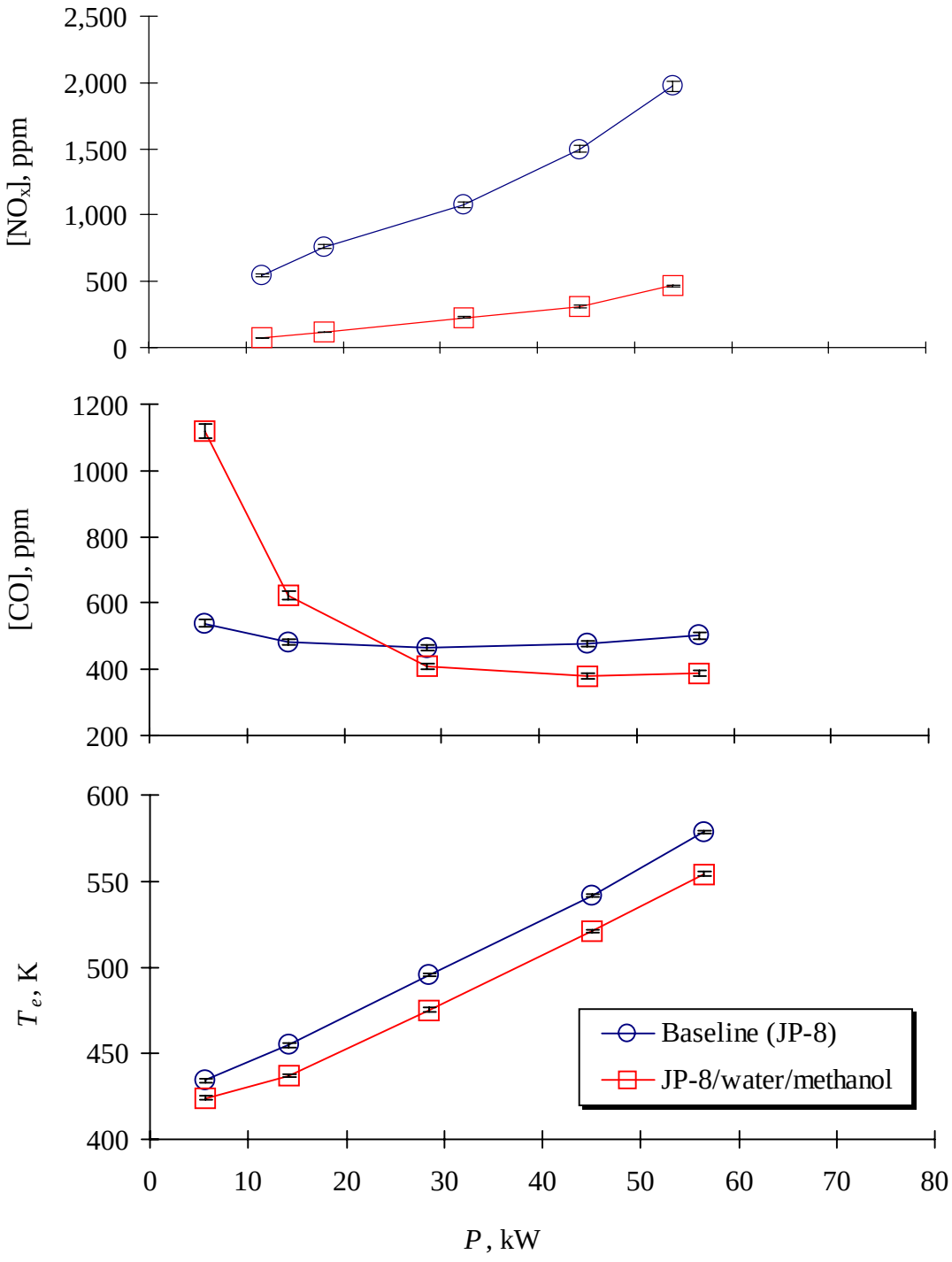

Figure 19: JP-8/water/methanol with N65 injectors at 3.769 cm

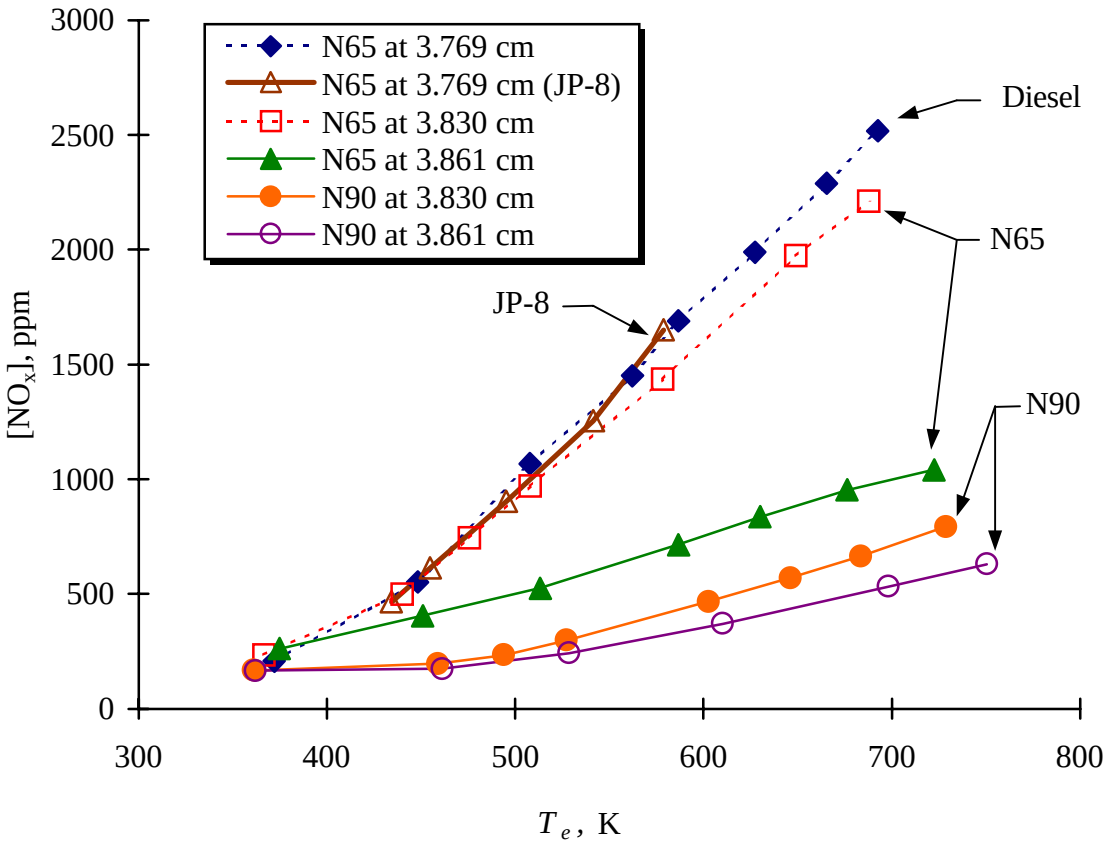

Figure 20: Baseline [NO_x] versus exhaust temperature for N65 and N90 injectors at various fuel injection delay settings

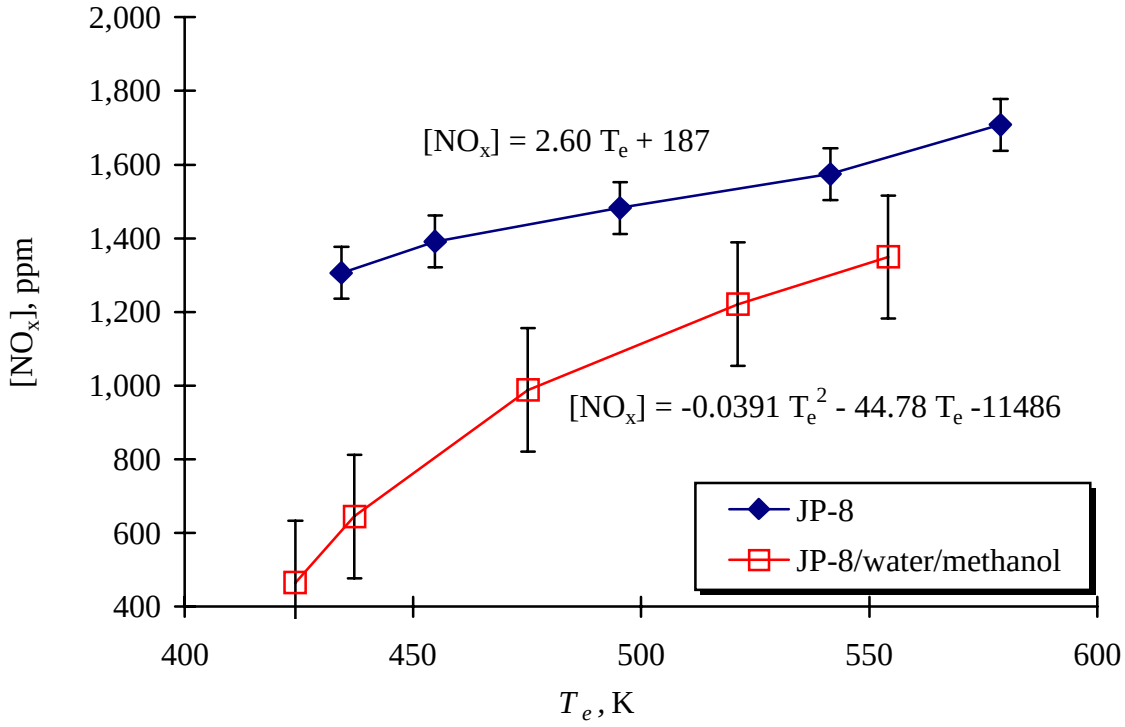

Figure 21: [NO_x] versus exhaust temperature for JP-8
and 65% JP-8 / 30% water / 5 %methanol (by volume) mixture

N90 Injectors

Figures 17 and 18 present data for the N90 injectors at 3.830 and 3.861 cm, respectively. The N90 injector was not tested at 3.769 cm because tests with the N65 injector at delayed timing settings resulted in significant NO_x reductions. Figure 17 shows baseline NO_x emissions of 659 ppm at 60 kW are reduced to 272 ppm with 45% water, a reduction factor of 2.42. Note that the generator would produce slightly less than 40 kW with the N65 injectors and 43% water (Figure 16), demonstrating the significance of increasing the injector size.

Comparing the exhaust temperatures at 60 kW, the baseline exhaust temperature of 683 K reduced to 625 K, a factor of 1.09. This is very comparable to the results using the N65 injector

(Figure 16), except we were able to attain 1.5 times the power output (60 kW versus 40 kW) with 1.05 times more water in the fuel (43 to 45%) using the N90 injector.

Figure 18 shows similar reductions in NO_x and exhaust temperature, although intermediate data were not taken at 30% water, only 40 and 45%. The exhaust temperature for the 45% water case is 1.028 times higher than the 40% water case, although lower NO_x, was measured. The significantly-lower CO for 40% water suggests that a variability between fuels, other than water content, may have occurred between the 40 and 45% mixtures reported. For example, a poorly-mixed 45% emulsion, in which the water ratio decreased with time, would account for the slightly higher exhaust temperature.

JP-8/Water/Methanol Tests

Data shown in Figure 19 was taken using a blend of 64% JP-8, 30% water, 5% methanol, and 1% additives, by volume. A new testing protocol was followed, in compliance with the International Organization for Standardization (ISO) testing procedures for compression ignition 2-stroke engines. The test cycle called for testing at load settings of 10, 25, 50, 75, and 100% full load. Based upon experience and preliminary testing, we established 56 kW as full load and then tested at the prescribed percentages. Please note that the injector and timing setting for data reported in Figure 19, N65 at 3.769 cm, corresponds to the diesel/water mixture injector and timing settings reported in Figure 16.

The NO_x reduction of 78% at 50 kW is substantially higher than the 44% reduction reported in previous tests (Figure 19). The CO emissions at low loads are also significantly lower in Figure 19 versus Figure 16. For example, CO emissions at 15 kW were 623 ppm for the JP-8/water/methanol mixture in Figure 19, versus 2826 ppm for the diesel/water mixture in Figure 16, a factor of 4.53. Possible explanations for this high variation in CO emissions include engine variabilities, differences in JP-8 versus diesel combustion, testing condition variables, and CO

monitoring equipment calibration. The most likely cause, demonstrated in recent studies, is the variability of NO_x and CO emissions across these diesel generator units. Data in Figure 16 were taken in late 1996 using a diesel generator no longer in service, whereas data in Figure 19 were recorded in late 1998 from a diesel generator fresh out of six-month maintenance. Several other engines tested in late 1998 also displayed high CO emissions and slightly higher NO_x emissions and were suspected to have poor cylinder compression. Testing conditions also varied: data in Figure 19 were recorded in mild Florida winter ambient temperature of 289 K, whereas data in Figure 16 were recorded in humid Florida summer with ambient temperatures of 308 K. Higher intake temperatures affect the volumetric efficiency and ignition delay of the compression ignition engine cycle.

NO_x reductions at lower loads are slightly higher. Exhaust temperatures for this fuel and engine test were 4.25% lower with the JP-8—water fuel. Measurable discrepancies exist across engines and future test programs will require the use of multiple engines.

Shown in Figure 20 are NO_x emissions versus temperature for the baseline case of all injector/timing settings tested. We must be careful interpreting results like those in Figure 20. As shown earlier, both NO_x and exhaust temperature increase with load setting on the generator. We have demonstrated through practice that thermal NO_x formation is significant in the subject diesel engine, but further correlation is required to prove the hypothesis that diesel—water emulsions lower the combustion flame temperature *and* suppress thermal NO_x formation.

Uncertainties

Error bars are plotted in Figure 19 to demonstrate the low level of instrument error in our tests. The [CO] and [NO_x] data accuracy is ±2 percent of indicated value, plotted in Figure 19 as positive and negative errors. The Omega thermocouples used to measure exhaust temperature, T_e, are accurate to ±1.0 K. These errors are also plotted in Figure 19.

NO_x Versus Exhaust Temperature

Combustion products and exhaust temperature to this point have been presented as a function of power load on the generator. Baseline NO_x emissions are plotted against the corresponding exhaust temperature in Figure 20. A strong trend exists for increased NO_x with increased exhaust temperature as fuel injector size increases and timing is delayed. Note the higher values and slope for N65 injectors versus N90 injectors at timing setting of 3.830 cm. Please also note the overlap for N65 injectors at 3.769 cm, with both diesel and JP-8 fuels, demonstrating the similarity between the fuels. The line labeled "JP-8" is repeated in Figure 21.

Figure 21 presents [NO_x] as a function of exhaust temperature for the recent investigations using JP-8 and the JP-8/methanol/water mixture with 30% water and 5% methanol, by volume. Trend line "JP-8" is repeated from Figure 20, along with data for the mixture, to compare how the NO_x formation as a function of temperature varies with the addition of water (and in this case methanol). Figures comparing each of the baseline trends in Figure 20 with its corresponding NO_x versus exhaust temperature trend have been not been included for the sake of brevity. Error bars are plotted in Figure 21 depicting the positive and negative standard error for each data series. The standard error for the JP-8 data set is lower due to smaller differences between data points. A clear trend is shown for increased NO_x emissions with increased exhaust temperature, both for the baseline case of JP-8 fuel and the JP-8/water/methanol mixture.

The linear curve-fit equations were plotted in Figure 21. It is interesting to note that while the y-intercept for the mixture is significantly lower, at –2280 ppm, than that for JP-8, 187 ppm, the slope for the mixture is 2.56 times that of the JP-8. The slope of the line can be interpreted as an empirical NO_x formation rate based upon exhaust temperature, with units of ppm/K.

First Law of Thermodynamics Calculation

The stoichiometry for fuel-lean combustion ($\phi \leq 1$) was described by Equation (5) in Chapter 2:

$$C_x H_y + a(O_2 + 3.76N_2) \rightarrow bCO_2 + dH_2O(g) + fO_2 + 3.76aN_2 \quad (5)$$

We will apply Equation (5) first to determine the adiabatic flame temperature of the baseline case for diesel fuel combustion:

Case 1: Diesel combustion

Given: Diesel fuel

Equivalence ratio, ϕ = 0.8

Temperature of reactants, T_R = 298 K

Pressure of reactants, p_R = 100 kPa

Find: Temperature of products (adiabatic flame temperature), T_P

Assumptions: Steady-state steady-flow process

Pressure of products, p_R = 100 kPa

Model diesel fuel as $C_{14.4}H_{24.9}$ (Sonntag et al.,1998)

Solution:

Please refer to first-law control volume around the combustion engine in Figure 7. Modeling diesel fuel as $C_{14.4}H_{24.9}$ and solving for the coefficients of Equation (5) per Equations (7) through (12) yields the following:

$$a = \frac{x + \frac{y}{4}}{\phi} = \frac{14.4 + \frac{24.9}{4}}{0.8} = 25.8 \quad (37)$$

$$b = x = 14.4 \quad (38)$$

$$d = \frac{y}{2} = \frac{24.9}{2} = 12.45 \tag{39}$$

$$f = (1-\phi)a = (1-0.8)(25.8) = 5.16 \tag{40}$$

Inserting these coefficients into Equation (5) yields:

$$\begin{gathered} C_{14.4}H_{24.9}(\ell) + 25.8(O_2 + 3.76N_2) \rightarrow \\ 14.4CO_2 + 12.45H_2O(g) + 5.16O_2 + 96.9N_2 \end{gathered} \tag{41}$$

Using Equation (13), with Q_{CV} = 0 and W_{CV} = 0, gives the following equality for the enthalpies of reactants and products:

$$\sum_R n_i \bar{h}_i = \sum_P n_j \bar{h}_j \tag{42}$$

The total reactant enthalpies can be evaluated according to the sum of the respective species' enthalpies of formation, $\bar{h}_f^\circ$, and the species' enthalpies, $\Delta\bar{h}$, at the reactant temperature and pressure:

$$H_R = \sum_R n_i (\bar{h}_f^\circ + \Delta\bar{h})_i \tag{43}$$

Evaluating Equation (43) for reactant molar balances in Equation (41), with enthalpies evaluated at T_R = 298K, p_R = 100 kPa, and enthalpies of formation from Sonntag et al. (1998), Table A.8, yields:

$$\begin{aligned} H_R &= \bar{h}_{f,C_{14.4}H_{24.9}}^\circ + 25.8\bar{h}_{f,O_2}^\circ + 96.9\bar{h}_{f,N_2}^\circ \\ &= -174{,}000 + 0 + 0 = -174{,}000\,\text{kJ/kmol} \end{aligned} \tag{44}$$

Please note that the respective $\Delta\bar{h}_i$ from Equation (43) are zero because we chose the reactant temperature and pressure equal to the reference state for enthalpy of formation.

Similarly, the equation for product enthalpy, substituting enthalpies of formation from Sonntag et al. (1998), Table A.8, is

$$\begin{aligned} H_P = \sum_P n_j (\bar{h}_f^\circ + \Delta\bar{h})_j &= 14.4\left(-393{,}522 + \Delta\bar{h}_{CO_2}\right) \\ &+ 12.45\left(-241{,}826 + \Delta\bar{h}_{H_2O(g)}\right) + 5.16\Delta\bar{h}_{O_2} + 96.9\Delta\bar{h}_{N_2} \end{aligned} \tag{45}$$

The flame temperature is now calculated using an iterative procedure to equate H_R and H_P using the product enthalpies $\Delta\bar{h}_{CO_2}$, $\Delta\bar{h}_{H_2O}$, $\Delta\bar{h}_{O_2}$, $\Delta\bar{h}_{N_2}$. These results are listed in Table 11 for product temperature from 1600 K to 2400 K.

Table 11: Adiabatic flame temperature iteration for diesel combustion

T_P, K	$\Delta\bar{h}_{CO_2}$	$\Delta\bar{h}_{H_2O}$	$\Delta\bar{h}_{O_2}$	$\Delta\bar{h}_{N_2}$	H_P, kJ/kmol	H_R, kJ/kmol
1600	67569	52907	44267	41904	-2756849	-174000
2000	91439	72788	59176	56137	-709495	-174000
2200	103562	83153	66770	63362	333408.2	-174000
2400	115779	93741	74453	70640	1386036	-174000

Note that the product enthalpy, H_P, passes the value of reactant enthalpy H_R between T_P = 2000 and 2200 K. Interpolating for the product temperature between 2000 and 2200 K yields

$$\boxed{T_P = 2102 \text{ K}}. \qquad (46)$$

Calculation of the adiabatic flame temperature for the diesel—water combustion case follows the same basic procedure, except the addition of water as a reactant must be included in the combustion equation, demonstrated below:

Case 2: Diesel—water combustion

Given: 70% diesel, 30% water (by volume) fuel

Equivalence ratio, ϕ = 0.8

Temperature of reactants, T_R = 298 K

Pressure of reactants, p_R = 100 kPa

Find: Temperature of products (adiabatic flame temperature), T_P

Assumptions: Steady-state steady-flow process

Pressure of products, p_R = 100 kPa

Model diesel fuel as $C_{14.4}H_{24.9}$ (Sonntag et al.,1998)

All water reactant goes to water product

Solution:

Determine the molar ratio of diesel and water for a 70/30 volumetric ratio, on a 1 m^3 basis, using density and molecular weight of water and diesel at reactant conditions, with diesel again modeled as $C_{14.4}H_{24.9}$:

$$\frac{N_{diesel}}{N_{water}} = \frac{\dfrac{0.7\,\mathrm{m^3\,C_{14.4}H_{24.9}}}{1\,\mathrm{m^3}}}{\dfrac{0.3\,\mathrm{m^3\,H_2O}}{1\,\mathrm{m^3}}} \times \frac{876\,\dfrac{\mathrm{kg}}{\mathrm{m^3}}}{997\,\dfrac{\mathrm{kg}}{\mathrm{m^3}}} \times \frac{\dfrac{1\ \mathrm{kmol}}{198.06\ \mathrm{kg}}}{\dfrac{1\ \mathrm{kmol}}{18.015\ \mathrm{kg}}} = \frac{1\ \mathrm{kmol\ C_{14.4}H_{24.9}}}{5.36\ \mathrm{kmol\ H_2O}} \tag{47}$$

Thus, for every 1 kmol of diesel there are 5.36 kmol of water in our fuel blend. Adding liquid water as a reactant to Equation (41) and balancing yields:

$$\begin{gathered} C_{14.4}H_{24.9}(\ell) + 5.36H_2O(\ell) + 25.8(O_2 + 3.76N_2) \rightarrow \\ 14.4CO_2 + 17.8H_2O(g) + 5.16O_2 + 96.9N_2 \end{gathered} \tag{48}$$

Summing the reactant enthalpies:

$$\begin{aligned} H_R &= \bar{h}^\circ_{f,C_{14.4}H_{24.9}} + 5.36\bar{h}^\circ_{f,H_2O(\ell)} + 25.08\bar{h}^\circ_{f,O_2} + 96.9\bar{h}^\circ_{f,N_2} \\ &= -174{,}000 + 5.36(-285{,}830) + 0 + 0 = -1{,}706{,}049\ \mathrm{kJ/kmol} \end{aligned} \tag{49}$$

Summing the product enthalpies:

$$\begin{aligned} H_P &= \sum_P n_j(\bar{h}^\circ_f + \Delta\bar{h})_j = 14.4\left(-393{,}522 + \Delta\bar{h}_{CO_2}\right) \\ &+ 17.8\left(-241{,}826 + \Delta\bar{h}_{H_2O(g)}\right) + 5.16\Delta\bar{h}_{O_2} + 96.9\Delta\bar{h}_{N_2} \end{aligned} \tag{50}$$

The iterative results are listed in Table 12 for product temperature from 1600 K to 2200 K.

Table 12: Adiabatic flame temperature iteration for diesel—water combustion

$T_{P,}$ K	$\Delta\bar{h}_{CO_2}$	$\Delta\bar{h}_{H_2O}$	$\Delta\bar{h}_{O_2}$	$\Delta\bar{h}_{N_2}$	H_P, kJ/kmol	H_R, kJ/kmol
1600	67569	52907	44267	41904	-3767566	-1706049
1800	79432	62693	51674	48979	-2698760	-1706049
1900	85420	67706	55414	52549	-2158070	-1706049
2000	91439	72788	59176	56137	-1613848	-1706049
2200	103562	83153	66770	63362	-515492	-1706049

The product enthalpy, H_P, passes the value of reactant enthalpy H_R between T_P = 1900 and 2000 K. Interpolating for the product temperature yields

$$\boxed{T_P = 1983\text{K}}\,. \tag{51}$$

Comparing the results from Cases 1 and 2, the adiabatic flame temperature dropped 119 K, from 2102 K to 1983 K, a factor of 1.060 or 5.7 %, when including the enthalpy required to convert liquid water in the fuel to water vapor. Before discussing these results from Cases 1 and 2 we will first examine the results provided by a computer code to determine the equilibrium products of combustion.

Equilibrium Code Calculation

The diesel and diesel—water combustion cases were also evaluated using the computer program HPFLAME provided in Turns (1996), based upon the equilibrium products of combustion code by Olikara and Borman (1975). HPFLAME calculates the adiabatic flame temperature, equilibrium products of combustion, and mole fractions of the primary product species for adiabatic constant-pressure combustion. As described in Chapter 2, the diesel

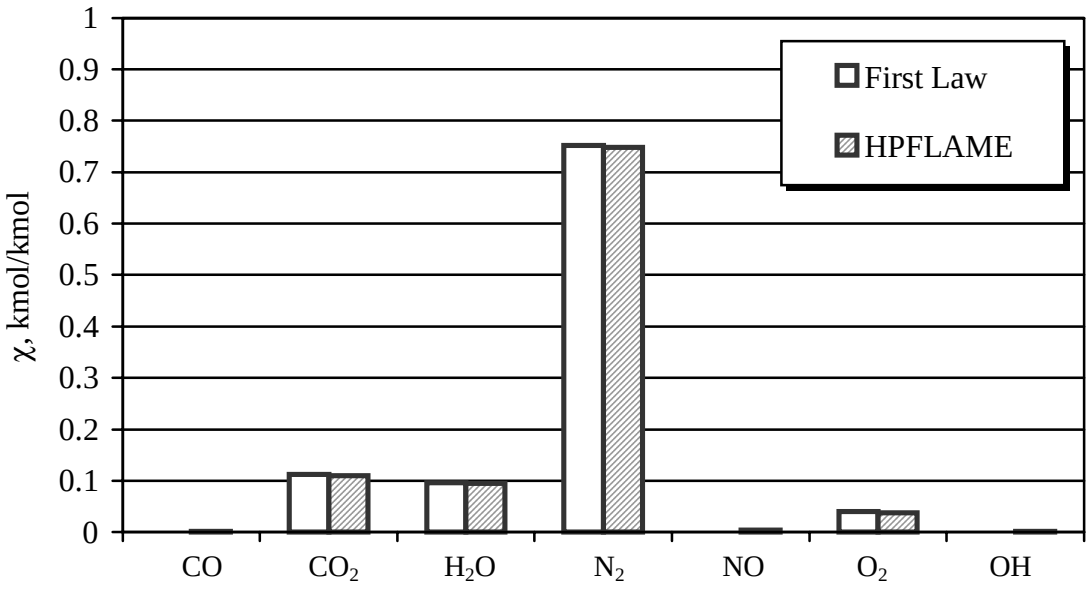

Figure 22: Diesel combustion product mole fractions χ for first law and HPFLAME calculations

combustion process can be approximated as adiabatic constant-pressure combustion. Turns (1996) also provides programs UVFLAME, for adiabatic constant-volume combustion (gasoline spark-ignition), and TPEQUIL for calculations when the combustion temperature is known.

Results for the analysis of the diesel fuel combustion, with the diesel fuel again modeled as $C_{14.4}H_{24.9}$, are presented in Table 13. The program requires the input of carbon, hydrogen, oxygen, and nitrogen atoms in the fuel, as well as the equivalence ratio, initial combustion temperature guess, pressure, and enthalpy of reactants. These inputs correspond to the previous evaluation of the reactant enthalpies in the Case 1.

Please note the additional inclusion of H, O, N, H_2, OH, CO, and NO beyond the first law evaluation in Case 1. OH, CO, NO, O_2, H_2O, CO_2, and N_2 account for over 99.9 % of all products, so H, O, N, and H_2 products will be neglected. HPFLAME estimated the adiabatic flame temperature at T_P = 2073 K, which is 29 K or a ratio of only 1.014 less than the first law result of 2102 K. The major mole fractions for the first-law analysis and HPFLAME are shown in Figure 22. Equilibrium mole fractions of for the first law calculation are simply the fraction of

individual product moles to total product moles from Equation (41) in Case 1. For example, summing product moles from Equation (41) yields 14.4 + 12.45 + 5.16 + 96.9 = 128.9 kmol, and mole fraction of N_2 is then $\frac{96.9}{128.9} = 0.752$ kmol/kmol. Figure 22 demonstrates there is a good correlation between the first-law analysis and the equilibrium products of combustion code for fuel-lean combustion diesel fuel combustion.

Shown in Table 14 are results for HPFLAME calculation of adiabatic flame temperature and equilibrium products of combustion for the case of diesel—water combustion, as described in Case 2. Note the inputs correspond to the enthalpy and reactant conditions from Case 2. Please also note that HPFLAME also allows input of O and N fuel molecules. As described earlier in Chapter 3, liquid fuels such as diesel, kerosene and gasoline contain little to no fuel-bound nitrogen. Nitrogen molecules in the fuel might be included if calculating the flame temperature for a coal-fired boiler. The inclusion of O molecules in the fuel would be treated by HPFLAME as an oxygenated fuel, so including additional H and O molecules for $H_2O(\ell)$ in the fuel would not be modeled properly. Turns (1996) included the source code for HPFLAME, in which the constituents of air are specified (79% N_2 and 21% O_2). An interesting project would be to modify the routines in HPFLAME to include kinetic pathway modeling for high concentrations of $H_2O(\ell)$ in the fuel.

For the diesel—water combustion case, HPFLAME estimated the adiabatic flame temperature at T_P = 1799 K, which is 184 K, or a ratio of 1.10 less than the first law result of 1983 K determined in Case 1. This variation is significantly greater than the 1.014 reduction ratio for the diesel fuel combustion calculations, further demonstrating the variation between the two methods for calculating diesel—water mixture combustion characteristics.

Table 13: HPFLAME results for diesel combustion

Inputs (Reactants)			
Carbon atoms			14.4
Hydrogen atoms			24.9
Oxygen atoms			0.0
Nitrogen atoms			0.0
Equivalence ratio, ϕ			0.800
Flame temperature guess, K			2000.0
Pressure, kPa			101.325
Enthalpy of reactants, kJ/kmol fuel			-174000.0
Results (Products)			
Adiabatic flame temperature, K			2073.61
Mixture enthalpy, kJ/kg			-46.54
Mixture specific heat, c_p, J/kg·K			1419.97
Specific heat ratio, c_p/c_v			1.2232
Mixture molecular weight, kg/kmol			28.9537
Moles of fuel per mole of products			0.00774456
Mole Fractions of Product Species			
H	0.00004084	NO	0.00410114
O	0.00022365	O_2	0.03810987
N	0.00000000	H_2O	0.09524323
H_2	0.00024079	CO_2	0.11018881
OH	0.00183075	N_2	0.74868802
CO	0.00133290		

Comparing results in Tables 13 and 14, HPFLAME calculates the adiabatic flame temperature to decrease from 2073 K to 1799 K, a factor of 1.15, or 13.2 %. This result is 1.08 times greater than the 1.060 factor flame temperature decrease calculated with the first law analysis from Cases 1 and 2. In other words, the equilibrium products calculated by HPFLAME predicts a lower flame temperature and greater percent flame temperature reduction than the first law analysis. The reason for this discrepancy can be seen by comparing the stoichiometric combustion products listed in Case 2, Equation (50). By estimating that all of the water in the fuel as a reactant goes to steam as a product, we were able to include the enthalpy of formation of

Table 14: HPFLAME results for diesel—water combustion

Inputs (Reactants)			
Carbon atoms			14.4
Hydrogen atoms			24.9
Oxygen atoms			0.0
Nitrogen atoms			0.0
Equivalence ratio, ϕ			0.800
Flame temperature guess, K			2000.0
Pressure, kPa			101.325
Enthalpy of reactants, kJ/kmol fuel			-1706049.0
Results (Products)			
Adiabatic flame temperature, K			1799.31
Mixture enthalpy, kJ/kg			-456.3
Mixture specific heat, c_p, J/kg·K			1419.97
Specific heat ratio, c_p/c_v			1.2540
Mixture molecular weight, kg/kmol			28.9883
Moles of fuel per mole of products			0.00775383
Mole Fractions of Product Species			
H	0.00000181	NO	0.00186311
O	0.00002369	O_2	0.03899801
N	0.00000000	H_2O	0.09628909
H_2	0.00002602	CO_2	0.11154139
OH	0.00043824	N_2	0.75070493
CO	0.00011370		

the $H_2O(g)$ on the RHS of the first-law balance. This accounts for the enthalpy required to convert the water to steam and slightly lowers enthalpy available for combustion. However, HPFLAME is treats the reduced reactant enthalpy, from –174,000 KJ/kg to –1,706,049 KJ/kg as a very low-heating value fuel, without estimating water in the products.

One benefit of applying HPFLAME to this study included the calculation of equilibrium concentrations of NO. Comparing equilibrium mole fractions for NO, designated χ_{NO}, from Tables 13 and 14, χ_{NO} decreased from 0.00410 to 0.00186 kmol/kmol. Thus, HPFLAME predicts

a 2.20 factor decrease in equilibrium NO production with the reduced reactant enthalpy. This suggests that lower heating-heating value fuels (or diluted high-heating value fuels) lower the flame temperature and reduce total NO production.

Figure 23 depicts the diesel—water combustion product molar fractions for the first law and HFPLAME calculations. Data for HPFLAME were taken from Table 14 and first law product mole fractions were calculated from Equation (48). The greater molar fraction for N_2 is likely the primary source of discrepancy between the two calculations. Recall that 5.36 kmoles of $H_2O(\ell)$ was added to the reactant in Equation (48), whereas in HPFLAME the sole input to account for the reactant composition, other than the fuel, was a reduced reactant enthalpy.

NO_x Formation Rate Calculation

Please recall the NO formation rate relationship, Equation (31):

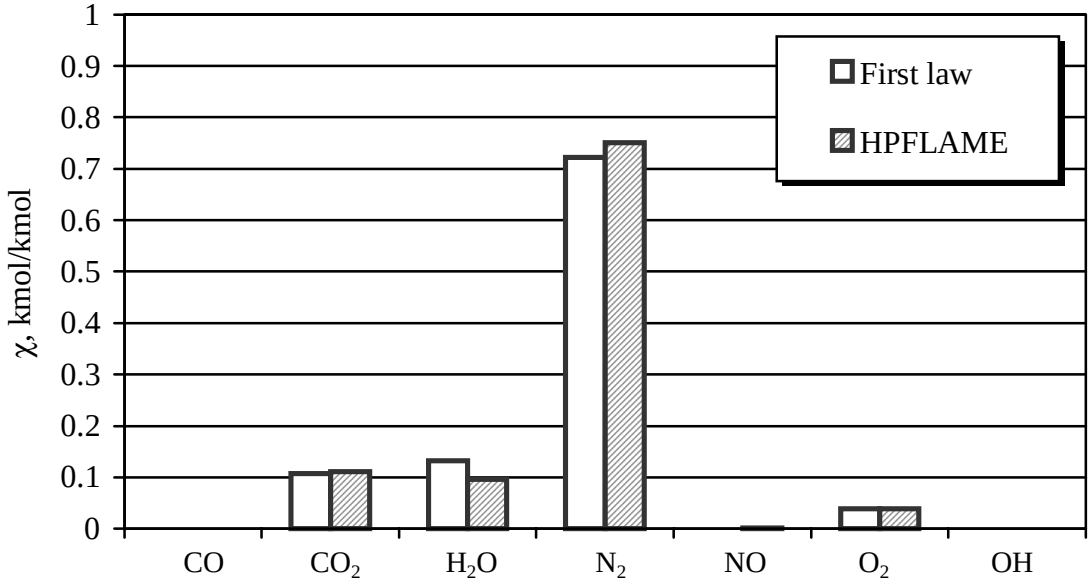

Figure 23: Diesel—water combustion product mole fractions χ for first law and HPFLAME calculations

$$\frac{d[NO]}{dt} = \frac{6\times10^{16}}{\sqrt{T}} e^{\left(\frac{-69,090}{T}\right)} [N_2]_e \sqrt{[O_2]_e} \quad (31)$$

It is more convenient to work with the mole fraction, χ_i. The molar concentration $[X_i]$ is related to the mole fraction as

$$[X_i] = \frac{\chi_i P}{\overline{R} T} \quad (52)$$

where $\overline{R}$ is the universal gas constant, 8.3145 kJ/kmol·K, and P and T are the adiabatic flame pressure and temperature. Substituting Equation (52), with P = 100,000 Pa, into Equation (31) yields

$$\frac{d\chi_{NO}}{dt} = \frac{6.58\times10^{18}}{T} e^{\left(\frac{-69,090}{T}\right)} \chi_{N_{2,e}} \sqrt{\chi_{O_{2,e}}} \quad (53)$$

Listed in Table 15 are the formation rates for diesel and diesel—water combustion using the NO formation rate relationships from Equation (53). Results are based upon adiabatic flame temperature and mole concentrations from the first law analysis, HPFLAME calculations, and correlations to exhaust temperature variations. First law product temperatures T_P are taken from Cases 1 and 2, and HPFLAME T_P were listed in Tables 13 and 14. Equilibrium product mole fractions $\chi_{O_{2,e}}$ and $\chi_{N_{2,e}}$ are taken from the data graphed in Figures 22 and 23. Please note that these results depict NO mole fraction production rate, which differs from the equilibrium NO mole fraction reported earlier for the HPFLAME calculation. Results depicted in Table 15 are

Table 15: NO production rate calculations

Fuel	Model	T_P, K	$\chi_{O_{2,e}}$	$\chi_{N_{2,e}}$	$\frac{d\chi_{NO}}{dt}, \frac{kmol}{kmol\cdot s}$	$\Delta\left(\frac{d\chi_{NO}}{dt}\right)$
Diesel	First law	2102	0.0400	0.752	2.50	
Diesel—water	First law	1983	0.0384	0.722	1.10	2.27
Diesel	HPFLAME	2073	0.0381	0.749	1.56	
Diesel—water	HPFLAME	1799	0.0390	0.751	0.011	142
Diesel	Exhaust	2102	*0.0400*	*0.752*	2.50	
Diesel—water	Exhaust	1932	*0.0384*	*0.722*	0.151	16.6

based upon flame temperature and equilibrium.

In summary, Equation (53) predicts NO mole fraction formation rate reduces 2.27, 142, and 16.6 times for diesel—water fuels, based upon data from the first law analysis, HPFLAME, and exhaust temperature calculations, respectively. The HPFLAME NO mole production rate is effectively zero for the diesel—water mixture. The greater reduction based upon HPFLAME data is a result of the calculated 274 K flame temperature reduction, versus 119 K and 170 K for the first law and exhaust temperature analyses, respectively. Additionally, the HPFLAME NO mole fraction formation rate for diesel combustion (1.56 kmol/kmol·s) is initially 1.6 times less than the first-law NO mole fraction formation rate (2.50 kmol/kmol·s). This is a result of the lower diesel combustion flame temperature and equilibrium O_2 and N_2 mole fractions for HPFLAME.

Correlating these results to our experimental data could be conducted by either correlating flame temperature to the exhaust temperature, or using relative exhaust temperature reductions, to evaluate NO production rate reductions via Equation (53). Taking the latter approach, we refer again to Figure 16 to compare the baseline diesel exhaust temperature to the diesel—water mixture exhaust temperature. At 50 kW, the exhaust temperature decreases from 620 K to 570 K, a -8.06% or 1.088 factor decrease. Applying this ratio to the adiabatic flame temperature calculated in Case 1 for diesel combustion, 2102 K, yields an estimated flame temperature for the diesel—water mixture of 1931 K. This result is also tabulated in Table 15. Please note in Table 15 that the first law and HPFLAME flame temperature reduction factors were 1.060 and 1.152, respectively. Again, our first law analysis appears to be more accurate, correlating to our experimental factor of 1.088 very closely. Equilibrium product mole fractions for oxygen and nitrogen, $\chi_{O_{2,e}}$ and $\chi_{N_{2,e}}$, are of secondary effect to temperature in Equation (53). Thus, $\chi_{O_{2,e}}$ and $\chi_{N_{2,e}}$ from the first law calculation were used for the exhaust temperature calculation. As shown in Table 15, using the experimentally observed exhaust temperature reduction, correlating it to an

equivalent flame temperature reduction, and applying the empirical relationship in Equation (53) yields a 16.6 factor decrease in NO mole fraction production rate.

Effects of Water Injection

Thermodynamic, physical, and chemical effects of water injection on the combustion process discussed here and in the literature can be summarized as follows:

1. Microexplosions accelerate the diffusion of combustion through the cylinder, decreasing the time required for combustion and increasing combustion efficiency
2. Water in the fuel decreases the heat content of the fuel, decreasing the energy output per mass of total fuel.
3. The partial pressure of water may accelerate the water—gas reaction (Sawa and Kajitani, 1992).

The effect of microexplosions of liquid water present in fuel is considered in the literature to be the primary mechanism for increasing combustion efficiency (Tsenev, 1983). Hsu (1986) conclusively measured slight ignition delay resulting from water added to diesel fuel, and attributed improved combustion to the delayed ignition improving the evaporation and mixing of the fuel.

The high heat of vaporization of water in the fuel has been demonstrated here to lower the adiabatic flame temperature. For individual engines and fuels there is a practical upper limit for percent by volume water in the fuel, after which combustion would be sufficiently slowed to significantly reduce the combustion efficiency. De Vita (1989) recommended an upper limit of 20 mass percent water in diesel, which corresponds to 45.5 volume percent water, to prevent increasing the brake specific fuel consumption (BSFC) of the engine. If slight increases in BSFC can be accepted, higher water ratios could be used.

Consideration is given in the literature to the extent that water added to the fuel modifies the chemistry of combustion, possibly through increasing OH, H, and O radical formation and

oxidation chemistry. Combustion chemistry is undoubtedly affected by the contribution of water to more-complete combustion, thus reducing the amount of unburned hydrocarbons and reducing eventual soot formation. Greeves et al. (1976) and others theorize that water vapor is generally present during combustion and that kinetic effects are distantly secondary to thermodynamic effects in reducing NO_x and soot formation. Following this line of reasoning can lead us to conclude that the theoretical results calculated from a first law of thermodynamics combustion balance and extended equilibrium products of combustion (HPFLAME) are representative of actual results, and that chemical effects can be neglected for global approximations.

CHAPTER 6

CONCLUSIONS AND RECOMMENDATIONS

Results

The summary in Table 15 shows a lower flame temperature and resulting lower production rate of NO is estimated by theory and was demonstrated by our experimental data. Our results confirm the reports in the literature by many other researchers (Table 6), that water addition to fuel lowers the flame temperature and suppresses thermal NO_x formation. using a four-stroke diesel-powered generator in common use by the U.S. Air Force,

A First Law of Thermodynamics calculation estimated a 1.06 factor decrease in adiabatic flame temperature from the baseline case of diesel only and a diesel—water mixture of 30 percent water, by volume. Equation (53) predicts a resultant 2.27 factor decrease in NO formation rate for the diesel—water mixture. An equilibrium products of combustion code corroborated the trend demonstrated by the first law calculation, with a 1.15 factor decrease in adiabatic flame temperature and a corresponding 142 factor decrease in NO formation rate. Experimental data shown in Figure 16 demonstrates this trend to decreased temperature, with exhaust temperature decreasing a factor of 1.09 at 50 kW with 30 percent water in the fuel.

Figure 16 and Figure 19 demonstrated similar results for diesel—water and JP-8—water mixtures, and Figures 17 and 18 demonstrated lower exhaust temperatures and NO_x emissions when delaying the fuel injection to the cylinder.

Conclusions

Our primary conclusion, which confirms the findings of researchers listed in Table 6 and the References, is that water added to fuel lowers the flame temperature and suppresses the formation of thermal NO_x in internal combustion engines. Our calculations estimated factor decreases of flame temperature of 1.06 and 1.15, with a corresponding NO formation rate decreases of 2.27 and 142, when adding water to fuel.

Our results also lead us to conclude that NO_x reduction from fuel injection timing delay and improved injector design, as demonstrated in Figure 15 and Figure 20, is also probably due to a reduced flame temperature. Figure 20 shows a trend to lower exhaust temperature and lower NO_x emissions with increased timing delay, which corresponds to the trend for water added to the fuel.

In general, we can conclude from the reported data that fuel—water mixtures are an effective option to reducing NO_x emissions from diesel engines without requiring modifications to the engine, if a lower full load is acceptable. By installing larger fuel injectors, the diesel engine can attain the original load level, as shown by Figure 17.

Recommendations for Further Study

Planned research includes further testing and refinement of the fuel emulsification additives. As shown by Montagne et al. (1987), adding surfactants to fuel can increase emissions of NO_x. To minimize both increased emissions and fuel costs due to surfactants, one should use the minimum level of surfactant necessary to stabilize the fuel—water mixture. A factorial analysis should be conducted varying fuel, water, surfactant, and other additive concentrations to determine first- and second-order effects.

The mixing time required to develop a stable emulsion is best determined empirically. Again, a factorial analysis varying the water and fuel ratios versus mixing power and time should be conducted to establish a matrix of mixing times required to guarantee a stable emulsion.

The need for a corrosion inhibitor should be quantified through visual and wear-metal testing on engine components after extended use of fuel—water blends both with and without a corrosion inhibitor. The added cost of the corrosion inhibitor should be firmly established and demonstrated as a necessity to protect the engine and components, not simply a precaution to subdue suspicions of corrosion potential. If a corrosion inhibitor is demonstrated as necessary, GC/MS analysis of exhaust emissions across all load ranges should be conducted to determine if corrosion inhibitor components are emitted from the engine. Worker safety concerns require monitoring to demonstrate that the xylene and ethylbenzene components common in corrosion inhibitors are fully combusted.

Ongoing investigations indicate difficulties in cold-start with the fuel mixtures containing water. Several factors likely contribute to this problem, including the lower heating value of the fuel when combined with water. When cooled, the water in the fuel raises the auto-ignition temperature of the fuel mixture. Initial tests indicate pre-warming the fuel is an effective option to enhance auto-ignition of the diesel—water emulsions. We recommend a test program to evaluate the temperature relationship, model the thermodynamic effects, and design and install a fuel tank heating unit on a diesel engine to improve cold-start.

APPENDIX

NOMENCLATURE

b	=	cylinder bore (diameter), mm
c_p	=	specific heat at constant pressure, J/kg·K
c_v	=	specific heat at constant volume, J/kg·K
h	=	enthalpy, kJ/kg
h_c	=	convective heat transfer coefficient, W/m^2·K
$\Delta\bar{h}$	=	change in enthalpy from reference state, kJ/kmol
$\bar{h}_f^\circ$	=	enthalpy of formation, kJ/kmol
k	=	thermal conductivity, W/m·K
$k_{N,f}$	=	forward rate coefficient for reaction N, m^3/kmol·s
$k_{N,r}$	=	reverse rate coefficient for reaction N, m^3/kmol·s
M	=	molecular weight, kg/kmol
$\dot{m}_f$	=	mass flow rate, kg/s
P	=	power, kW
p	=	pressure, kPa
Q_{LHV_V}	=	lower heating value at constant volume, kJ/kg
Q_{LHV_p}	=	higher heating value at constant pressure, kJ/kg
q''	=	heat flux, W/m^2

q''_{COND} = conductive heat flux, W/m^2

q''_{CONV} = convective heat flux, W/m^2

q''_{RAD} = radiative heat flux, W/m^2

$\overline{R}$ = universal gas constant, 8.3145 kJ/kmol·K

r_c = compression ratio, m^3/m^3

s = specific entropy, kJ/kg·K

T = temperature, K

T_e = exhaust temperature, K

W_{CV} = work done on control volume, kJ

Greek Symbols

ε = emissivity, $0 \leq \varepsilon \leq 1$

ρ = density, kg/m^3

σ = Stefan-Boltzman constant, 5.67×10^{-8} $W/m^2 \cdot K^4$

v = specific volume, m^3/kg

$[X_i]$ = molar concentration, ppm

χ_i = mole fraction

$\frac{d\chi_i}{dt}$ = mole fraction production rate, $kmol \cdot s^{-1}/kmol$

REFERENCES

Abdel-Rahman, A.A., 1998, "On the Emissions from Internal-Combustion Engines: A Review," *Int. J. Energy Res.*, Vol. 22, pp. 483-513.

Afify, E.M., 1985, "Performance Combustion Characteristics and Exhaust Emission of a Direct Injection Diesel Engine Using Water/Oil Emulsions as a Fuel," DTIC No. ADA-161-652, U.S. Army Research Office, Research Triangle Park, NC.

Afify, E.M., Korah, N.S., and Dickey, D.W., 1987, "The Effect of Air Charge Temperature on Performance, Ignition Delay and Exhaust Emissions of Diesel Engines Using W/O Emulsions as Fuel," SAE Paper 870555.

Akridge, R.J., Donegan, B.M., Rolader, G.E., Bienvenue, D.R., Verge, R.E., and Elliot,D., 1997, "Reduction of Nitrogen Oxides Emitted by Aerospace Ground Equipment at March ARB," Paper No. 97-TA36A.01, Proceedings of the Air & Waste Management Association's 90th Annual Meeting & Exhibition, June 8-13, 1997, Toronto, Ontario, Canada.

Andrews, G.E., Bartle, S. W., Pang. S.W., Nurein, A.M., and Williams, P.T., 1989, "Diesel/Water Emuslions: Influence on Ignition Delay and Emissions," Spalding, D. Brian and Afgan, N.H., ed. *Heat and Mass Transfer in Gasoline and Diesel Engines*, Proceedings of the International Centre for Heat and Mass Transfer, No. 26, Hemisphere Publishing Corp., New York, NY, pp. 613-625.

Antonov, V.N., 1983, "Features of Preparation of Water-Fuel Emulsions for Diesel Engines," *Chemistry and Technology of Fuels and Oils*, Vol. 19, No. 11-12, pp. 606-609.

Avallone, E.A. and Baumeister III, T, 1996 *Marks' Standard Handbook for Mechanical Engineers*, 10th Ed., McGraw-Hill, Inc., New York, NY.

Borman, G.L. and Ragland, K.W, 1998, *Combustion Engineering*, McGraw-Hill, Inc., New York, NY.

Campbell, A.S, 1979, *Thermodynamic Analysis of Combustion Engines*, John Wiley & Sons, New York, NY.

Canfield, C.A, 1996, "NOx Control for Aircraft and Aircraft Support Operations," Proceedings of the Second Annual Strategic Environmental Research and Development Program (SERDP) Symposium, December 1996, Tyson's Corner, VA.

Canfield, C.A. and Wander, J.D, 1996, "Applications of Non-Thermal Plasmas for Control of NOx and VOCs from U.S. Air Force Operations," Proceedings of the International Workshop on Plasma Technologies for Pollution Control and Waste Treatment, Beijing China, May 1996, Beijing Institute of Technology.

Canfield, C.A., Babyak, R.A., and Wander, J.D., 1997, "Demonstration of a Filter Cart for NOx Removal from Ground Support Equipment," Technical Report No. AL/EQ-TP-1997-0001, U.S. Air Force Research Laboratory, Tyndall AFB, FL.

Coon, C.W., Jr., 1981, "Multi-Cylinder Diesel Engine Tests with Unstabilized Water-in-Fuel Emulsions," SAE Technical Paper 810250.

Corbitt, R.A., 1990, *Standard Handbook of Environmental Engineering*, McGraw-Hill, Inc., New York, NY.

Crookes, R.J., Nazha, M.A.A., and Kiannajad, F., 1990, "A Comparison of Ignition and Emissions Characteristics for Alternative Diesel Fuels and Emulsions," *I. Mech. E. Seminar*, pp. 47-52.

De Vita, A., 1989, "Multi-Cylinder D.I. Diesel Engine Tests with Unstabilized Emulsion of Water and Ethanol in Diesel Fuel," SAE Paper 890450.

Dryer, F.L., 1975, "Fundamental Concepts on the Use of Emulsions as Fuels," West and Central States Sect, Joint Spring Meeting, San Antonio TX, Apr 1975, Combustion Institute.

Dryer, F.L., 1976, "Water Addition to Practical Combustion Systems –Concepts and Applications," 16th Symposium (Intl.) on Combustion, Cambridge MA, Aug 1976, Combustion Institute.

Durand, G.P. and Montgomery, J.D., 1995, "Source Test Report: Development of Emission Factors for Nitrogen Oxides, Sulfur Dioxide, Carbon Monoxide, Nonmethane Hydrocarbons, and Particulate Matter for Selected Aircraft Ground Equipment at March Air Force Base, California," U.S. Air Force Armstrong Laboratory, AL/OEBE, Brooks AFB TX.

Ekert, E.R.G. and Drake, Jr., Robert M, 1987, *Analysis of Heat and Mass Transfer*, Hemisphere Publishing Corp., New York, NY.

Energy Efficiency Systems, Inc., 1995, "ENERAC Integrated Emissions System Model 3000 Instruction Manual," Revision 6, December 1995, Westbury, NY.

Estefan, R.M., and Brown, J.G., 1990, "Evaluation of Possible Methanol Fuel Additives for Reducing Engine Wear and/or Corrosion," SAE Paper 902153, Methanol Fuel Formulations and In-Use Experiences, SP-840, pp. 17-39.

Federle, S.P., Wander, J., Rogers, J., Nejezchleb, A., and Canfield, A., 1998, "A Non-Thermal Plasma Discharge Based Exhaust Gas Treatment System for the A/M32A-86 Diesel Powered Generator," Technical Report No. AFRL-MN-EG-TR-1998-7085, AFRL/MNMW, Eglin AFB, FL.

Fujita, N., Nagahura, K., and Tsunokake, S., 1987, "The Effect of Gas Oil-Water-Methanol Emulsified Fuel on Diesel Engine Performance," Trans. of the Japan Society of Mechanical Engineers, Vol. 53, No. 486, pp. 654-658.

Ganesan, V, 1996, *Internal Combustion Engines*, McGraw-Hill, Inc., New York, NY.

Greeves, G., Khan, I.M., and Onion, G., 1976, "Effects of Water Introduction on Diesel Engine Combustion and Emissions," Proceedings, 16th Annual Symposium (Int.) on Combustion, Williams & Wilkins Co., pp. 321-336.

Herbstman, S. and Virk, K., 1989, "Effect of Diesel Fuel Composition and Additives on the Buildup of Injector Deposits," SAE Technical Paper 892119, Proceedings, International Fuels and Lubricants Meeting and Exposition, pp. 25-40.

Heywood, J.B., 1988, *Internal Combustion Engine Fundamentals*, McGraw-Hill, Inc., New York, NY.

Hsu, B.D., 1986, "Combustion of Water-in-Diesel Emulsion in an Experimental Medium Speed Diesel Engine," SAE Paper 860300

Johnson, R.T. and Stoffer, J.O., 1983, "Single Cylinder Engine Evaluations of Stabilized Diesel Fuels Containing Alcohols," SAE Paper 830559, Alternate Fuels for Spark Ignition and Diesel Engines, SP-542, pp. 105-121.

Kays, W.M., 1989, "Heat Transmission from the Engine to the Atmosphere," Spalding, D. Brian and Afgan, N.H., ed. *Heat and Mass Transfer in Gasoline and Diesel Engines*, Proceedings of the International Centre for Heat and Mass Transfer, No. 26, Hemisphere Publishing Corp., New York, NY.

Larsen, C., Oey, F., and Levendis, Y.A., 1996, "An Optimization Study of the Control of NOx and Particulate Emissions from Diesel Engines," SAE Paper 960473.

Lavoie, G.A., Heywood, J.B., and Keck, J.C., 1970, "Experimental and Theoretical Investigation of Nitric Oxide Formation in Internal Combustion Engines," *Combustion Science Technology*, Vol. 1, pp. 313-326.

Lebedev, O.N., and Nosov, V.P., 1980, "Efficiency of Use of Water-Fuel Emulsions in Medium-Speed Marine Diesels," *Chem. Tech. Fuels Oils*, Vol 16, No. 11-12, pp. 738-740.

Liu, Z., Xu, S., and Deng, B, 1993, "A Study of Methanol-Gasoline Corrosivity and its Anticorrosive Agent," Proceedings, 10th International Symposium on Alcohol Fuels, Nov. 1993, Colorado Springs, CO.

Marelli, E., 1995, "Diesel Fuel Emulsion," U.S. Patent 5,445,656, United States Patent and Trademark Office.

Montagne, X., Herrier, D., and Guibet, J.-C., 1987, "Fouling of Automotive Diesel Injectors—Test Procedure, Influence of Composition of Diesel Oil and Additives," SAE Paper 872118.

Moran, M.J. and Shapiro, H.N, 1988, *Fundamentals of Engineering Thermodynamics*, John Wiley & Sons, Inc., New York, NY.

Murayama, T., Morishama, Y., Tsukahara, M., and Miyamoto, N., 1978, "Experimental Reduction of NOx, Smoke, and BSFC in a Diesel Engine Using Uniquely Produced Water (0-80%) to Fuel Emulsion," SAE Paper 780224.

Nagese, K. and Funatsu, K., 1990, "A Study of NOx Generation Mechanism in Diesel Exhaust Gases," SAE Paper 901615.

Nakatsuji, T., Yasukawa, K., Tabata, K., Ueda, K., and Niwa, M., 1998, "Catalytic Reduction System of NOx in Exhaust Gases from Diesel Engines with Secondary Fuel Injection," *Applied Catalysis B: Environmental*, Vol. 17, pp. 333-345.

Obert, E.F., 1973, *Internal Combustion Engines and Air Pollution*, Harper & Row Publishers, Inc., New York, NY.

Olikara, C. and Borman, G.L., 1975, "A Computer Program for Calculating Properties of Equilibrium Combustion Products with Some Applications to I.C. Engines," SAE Paper 750468.

O'Neal, G.B., Storment, J.O., and Waytulonis, R.W., 1981, "Control of Diesel Exhaust Emissions in Underground Coal Mines—Single Cylinder Engine Experiments with Modified and Non-Conventional Fuels," SAE SP-495, Diesel Combustion and Emission Part 3, Int. Off-Highway Meeting & Exposition, Milwaukee, WI, pp. 13-23.

Peter-Hoblyn, J.D., and Valentine, J.M., 1996, "Reduction of Nitrogen Oxides Emissions from Vehicular Diesel Engines," U.S. Patent 5,584,894, United States Patent and Trademark Office.

Peter-Hoblyn, J.D., Valentine, J.M., and Dubin, L., 1998, "Enhanced Lubricity Diesel Fuel Emulsions for Reduction of Nitrogen Oxides," U.S. Patent 5,743,922, United States Patent and Trademark Office.

Pischinger, R., 1987, "The Importance of Heat Transfer to IC Engine Design and Operation," Spalding, D.B., editor, *Heat and Mass Transfer in Gasoline and Diesel Engines*, Proceedings of the International Centre for Heat and Mass Transfer, No. 26, Hemisphere Publishing Corp., New York, NY.

Ramos, J.I., 1989, "Mathematical Models of Diesel Engines," Markatos, N.C., ed, Computer Simulations for Fluid Flow, *Heat and Mass Transfer, and Combustion in Reciprocating Engines*, Proceedings of the International Centre for Heat and Mass Transfer, No. 27, Hemisphere Publishing Corp., New York, NY.

Rolader, G.E., Rogers, J.W., Nejezchlab, A.J., Federle, S.P., Littrell, D.M., Wander, J., and Canfield, C.A, 1997, "Non-Thermal Plasma Discharge Based NOx Removal System for Diesel Engine Exhaust," Paper No. 97-MP5.07, Proceedings of the Air & Waste Management Association's 90th Annual Meeting & Exhibition, June 8-13, Toronto, Ontario, Canada.

Sawa, N., and Kajitani, S., 1992, "Physical Properties of Emulsion Fuels (Water/Oil-Type) and Its Effect on Engine Performance under Transient Operation," SAE Paper 920198, International Congress & Exposition, Detroit MI.

Schwab, S.D., 1997, "Emulsion Diesel Fuel Composition with Reduced Emissions," U.S. Patent 5,669,938, United States Patent and Trademark Office.

SM-ALC/TISEA, 1986, "Technical Manual, Operator/Crew Organizational Maintenance Manual: Generator Set, Diesel Engine Driven, Wheel Mtd., 72kW 3 Phase, 4 Wire, 115/200 Volts," Technical Order No. 35C2-3-469-1, McClellan AFB, CA.

Smith, E.J. and Jordan, D.R., 1983, "The Use of Surfactants in Preventing Phase Separation of Alcohol Petroleum Fuel Mixtures," SAE Paper 830385, Alternate Fuels for Spark Ignition and Diesel Engines, SP-542, pp. 37-42.

Tsenev, V.A., 1983, "Features of Diesel Operation on Water—Fuel Emulsions," Translated from Khimiya I Tekhnologiya Topliv I Masel, No. 12, pp. 12-14.

Turns, S.R., 1996, *An Introduction to Combustion: Concepts and Applications*, McGraw-Hill, Inc., New York, NY.

Ulrich, A. and Kessler, A., 1992, "Method and Apparatus for Producing a Water-in-Fuel-Emulsion and Emulsifier-Free Water-in-Fuel-Emulsion," U.S. Patent 5,125,367, United States Patent and Trademark Office.

Urbach, H.B., Knauss, D.T., Emory, J., Wallace, B.L, Wasser, J.A., Sexton, M.R., and Frese, J., 1997, "The Reduction of NOx Emissions from Marine Power Plants," Paper No. 97-MP5.08, Proceedings of the Air & Waste Management Association's 90th Annual Meeting & Exhibition, June 8-13, 1997, Toronto, Ontario, Canada.

U.S. Department of Defense, 1995, "Military Specification Fuel, Naval Distillate", Naval Sea Systems Command, Washington D.C., Specification No. MIL-F-16884J.

U.S. EPA, 1995, "Determination of Nitric Oxide, Nitrogen Dioxide and NO_x Emissions from Stationary Sources by Electrochemical Analyzer," Emission Measurement Center (EMTIC), Technical Support Division, Office of Air Quality Planning and Standards, Research Triangle Park, NC.

Valdmanis, E. and Wulforst, D.E., 1970, "The Effect of Emulsified Fuels and Water Induction on Diesel Combustion," SAE Paper 700736.

Vichnievsky, R., 1975, "Use of Water-Fuel Emulsions in Diesel Engines," 11th Congress (Int) on Combustion, Barcelona Spain, May 1975.

Westbrook, C.K., and Dryer, F.L., 1981, "Chemical Kinetics and Modeling of Combustion Processes," 18th Symposium (Int.) on Combustion, Waterloo, Ontario, Canada, pp. 749-767: The Combustion Institute.

Yanagihara, H., 1997, "Simultaneous Reduction of NOx and Soot in Diesel Engines Using a New Mixture Preparation Method," *JSME International Journal*, Series B, Vol. 40, No. 4, pp. 592-598.

Yoshihara, S., Okabe, M., and Nakamaura, T., 1996, "Water Injecting Type Diesel Engine," U.S. Patent 5,522,349, United States Patent Office.

Yoshimoto, Yasufumi, Tsukarhara, Minoru, Muryama, and Tadashi, 1989, "Studies on the Microexplosion of Emulsified Fuels," *Nippon Kikai Gakkai Ronbunshun B Hen*, Vol. 55, No. 519, pp. 3538-3543.

Zhou, Q.-B., Wei, X.-Y., Zhu, T.-Z., 1987, "Radiation Heat Transfer in DI Diesel Engines," Spalding, D.B., editor, Heat and Mass Transfer in Gasoline and Diesel Engines, Proceedings of the International Centre for Heat and Mass Transfer, No. 26, Hemisphere Publishing Corp., New York, NY.

BIOGRAPHICAL SKETCH

Charles Alan Canfield was born at Chanute AFB, Illinois, and raised in Independence, Missouri. While attending the University of Missouri-Columbia, he was active in the Engineer's Club, Pi Kappa Alpha fraternity, and held an engineering internship with the 3M Corporation. Mr. Canfield received his Bachelor of Science in mechanical engineering in December 1991.

Mr. Canfield has been employed by Applied Research Associates, Inc. at Tyndall AFB, Florida, since 1993, supporting research programs for the Air Force Research Laboratory Airbase & Environmental Technologies Division. He is presently conducting catalytic studies with an advanced plug-flow annular reactor system. Currently the President of the Gulf Coast Chapter of the Florida Engineering Society, a state society of the National Society of Professional Engineers, he is a registered Professional Engineer in Florida. He is also a member of the Board of Advisors of the Gulf Coast Community College Civil Engineering Technologies Department, the Board of Directors of Girls Inc., and active in the Bay County Chamber of Commerce.

Upon completion of the Master of Science degree, Mr. Canfield will pursue studies in coordination with his in-house catalytic reaction engineering research. The research reported herein will be continued if sufficient funding and time is appropriated. Additional courses in chemistry and kinetic modeling will be pursued to enhance the understanding of the combustion process.

Mr. Canfield's past-times include road cycling and distance running, beach volleyball, working on his house and yard, keeping his old truck running, and collecting engineering references and textbooks.